Probing metabolism in an *E. coli*-based cell-free system reveals a trade-off between transcription and translation

Manisha Kapasiawala,[1*] Richard M. Murray,[1,2]

[1]Bioengineering, California Institute of Technology, Pasadena, CA, USA
[2]Control and Dynamical Systems, California Institute of Technology, Pasadena, CA, USA

[*]To whom correspondence should be addressed; E-mail: mkapasia@caltech.edu

Abstract

Cell-free transcription-translation (TX-TL) systems have been used for diverse applications, from prototyping gene circuits to providing a platform for the development of synthetic life, but their performance is limited by issues such as batch-to-batch variability, poor predictability, and limited lifetime. These issues stem largely from the fact that cell lysate contains an active and complex metabolism whose effect on TX-TL has remained largely uncharacterized.

Motivated by a minimal model of cell-free metabolism, this work explored the effects of energy molecules, which power TX-TL, and fuel molecules, which regenerate energy by harnessing core metabolism, on an *E. coli*-based TX-TL system. This work reports a compensatory interaction between TX-TL components Mg^{+2} and 3-phosphoglyceric acid (3-PGA, used to regenerate ATP), where if one component's concentration is increased, the other's must likewise be increased to maintain optimal translation. Furthermore, maximum total mRNA and protein production occur in different and opposite concentration regimes of Mg^{+2} and 3-PGA. To explore the observed phenomenon, transcription and translation were decoupled. Under translation inhibition, transcriptional output was uniform across Mg^{+2} and 3-PGA concentrations, but in a translation-only system, maximum protein production occurred in the previously found optimal regime of Mg^{+2} and 3-PGA, suggesting a TX-TL trade-off. Using alternative fuels to regenerate energy, this work found that the trade-off is universal across the different fuel sources, and that a system's position along the trade-off is determined strongly by Mg^{+2} and DNA concentrations. In systems where additional energy is supplied and where a fuel source is absent, the trade-off is absent, suggesting the trade-off arises from limitations in the regulation of translation and efficient energy regeneration. This work represents a significant advancement in understanding the effects of fuel and energy metabolism on TX-TL in cell-free systems and lays the foundation for improving TX-TL performance, lifetime, standardization, and prediction.

1 Introduction

Over the past few decades, synthetic biology has become a prominent interdisciplinary field that combines the principles of traditional engineering with the flexibility of biology to understand and engineer biological systems. Among the field's various focus areas, cell-free synthetic biology is a rapidly growing field that leverages the power of synthetic biology tools and techniques to engineer biological systems outside of living cells [11]. The cell-free approach offers several advantages over traditional cellular systems, including greater control over the reaction environment, the ability to produce toxic small molecules or proteins that are difficult to express in living cells, and scalability for biomanufacturing and other applications. In recent years, cell-free systems have become an important tool for protein engineering, structural biology, and drug discovery, enabling production of functional proteins such as enzymes, antibodies, and vaccine candidates [5, 11]. More broadly, cell-free systems have been used for applications such as rapid and high-throughput prototyping of engineered biological components and systems [15, 17, 30, 29, 34], biosensing and diagnostics [25, 37, 21], and the development of synthetic life [8, 36].

One of the most widely used applications of cell-free systems is cell-free protein synthesis, where crude cell lysates or purified proteins are supplemented with a DNA template and an energy buffer containing the molecular components that allow for *in vitro* transcription and translation (TX-TL) [28]. While cell lysates derived from *E. coli* are most commonly used, due to being well-characterized and enabling high-yield protein production, lysates from other cell types can also be used – including wheat germ, CHO, *Drosophila*, *Arabidopsis*, and HeLa cells – depending on the desired application [12]. Protein synthesis Using Recombinant Elements (PURE) has also been utilized, offering better predictability as a system with known composition, but its high production cost and limited scope have restricted its current use to simple proteins [26].

Although cell lysate-based TX-TL systems have many uses, their performance and applications are limited by issues such as batch-to-batch variability [9], lack of predictability for complex circuits [23], and limited lifetime [24]. These issues arise from the fact that cell lysate contains many proteins that are not necessary for cell-free protein synthesis. While some of these proteins have been used to regenerate energy molecules, most of them are irrelevant or even harmful for cell-free protein synthesis. The fraction of resources that are effectively utilized for TX-TL versus utilized to make

benign or possibly toxic by-products remains unknown.

1.1 Experimental efforts aimed at improving TX-TL characterization

To address these concerns, previous studies have sought to gain insight into TX-TL dynamics through a variety of approaches. Experimental studies have focused on how perturbations in TX-TL reaction conditions – including salts [14], fuel sources [16, 35], crowding agents [14, 32], and more [1, 3, 4, 7, 20, 24] – affect TX-TL performance. Additional studies have focused on the effects of factors such as cell lysate preparation methods [14], DNA preparation methods [14], and the presence of dialysis for semi-continuous or continuous TX-TL reactions [12]. Recently, some studies have harnessed lab automation and machine learning approaches in conjunction with experiments to rapidly optimize TX-TL systems [4, 6]. While experimental performance of a TX-TL system has historically been measured by final protein yields (concentration), recent efforts have expanded these performance metrics to include the maximum rate of protein production, the time to reach steady state protein level, and other characteristics of TX-TL dynamics and, in parallel, have investigated the effects of different TX-TL reaction conditions on these metrics [1].

1.2 Characterization efforts with a focus on cell-free metabolism

More recently, studies have focused on identifying and measuring the small molecules that participate in cell-free metabolism and studying their effects on TX-TL. Varner and co-workers have focused on combining modeling and experimental approaches to create a TX-TL model coupled with cell-free metabolism [13, 33]. Using dynamic measurements of nucleotide triphosphates (NTPs), amino acids, and several key metabolites of central carbon metabolism, they were able to construct an ensemble of kinetic models that could predict expression of a reporter protein, although the scalability of their approach in predicting protein expression dynamics for more complex circuits or different reaction conditions remains uncertain. A more recent paper by Miguez and co-workers used metabolomics to characterize and compare central carbon and amino acid metabolism under various reaction conditions, including the absence/presence of TX-TL, targeted supplementation of metabolic enzymes, and different methods of cell lysate preparation [19]. While this study also took a detailed approach towards metabolism, the implications for TX-TL prediction and lifetime extension were unclear.

Recent efforts by Poole and co-workers focused on efforts grounded in analytical chemistry to characterize *E. coli* cell-free metabolism via time-course measurements of hundreds of small molecules in *E. coli* cell lysates (metabolomics) during cell-free TX-TL [22]. The presence of these molecules, which are not added directly to the TX-TL reaction but rather generated through the metabolism of added TX-TL reaction components, suggested that the majority of *E. coli* metabolism is active during, and largely unaffected by, TX-TL at low concentrations of DNA. Next, Poole and co-workers used these insights, along with high-throughput TX-TL experiments and Bayesian parameter inference, to parametrize and validate a coarse-grained model of cell-free metabolism to predict cell-free TX-TL dynamics [22]. This model relied on a new experimental insight that the build-up of metabolic waste products plays a greater role in determining TX-TL lifetime than the depletion of energy molecules and other necessary substrates.

Poole's work provided a simple, generalizable framework that could be applied to characterize and predict the metabolism of any TX-TL system. However, the framework's ability to be adapted for different reaction systems was not reliably demonstrated. For example, could the model by applied to TX-TL systems where the fuel used to regenerate energy was phosphoenolpyruvate (PEP) or glucose instead of 3-PGA? Furthermore, how could the insight that there is a trade-off between energy regeneration and waste accumulation via fuel metabolism help to guide efforts aimed at reducing TX-TL variability or extending TX-TL lifetime?

Furthermore, the study only fit a model to predict the protein expression dynamics of deGFP with its gene under a constitutive promoter; it did not describe any attempts to more accurately predict protein expression in the presence of regulatory networks such as gene circuits, nor did it predict transcription dynamics.

Finally, while other studies have noted that the concentration of magnesium ions, Mg^{+2}, whose concentration widely varies across lab-to-lab formulations of TX-TL reactions, significantly affects TX-TL dynamics [1, 18, 20, 32], the model did include Mg^{+2}, perhaps owing to the difficulty of modeling species with electrostatic interactions, in addition to allosteric or catalytic functions.

Motivated by Poole's model of cell-free metabolism, this work explored the effects of energy molecules, which power TX-TL, and fuel molecules, which regenerate energy by harnessing core metabolism, on an *E. coli*-based TX-TL system. This work reports a compensatory interaction between TX-TL components Mg^{+2} and 3-Phosphoglyceric acid (3-PGA, used to regenerate ATP),

where if one component's concentration is increased, the other's must likewise be increased to maintain optimal translation. Furthermore, maximum total mRNA and protein production occur in different and opposite concentration regimes of Mg^{+2} and 3-PGA. To explore the observed phenomenon, transcription and translation were decoupled. Under translation inhibition, transcriptional output was uniform across Mg^{+2} and 3-PGA concentrations, but in a translation-only system, maximum protein production occurred in the previously found optimal regime of Mg^{+2} and 3-PGA, suggesting a TX-TL trade-off. Using alternative fuels to regenerate energy, this work found that the trade-off is universal across the different fuel sources, and that a system's position along the trade-off is determined strongly by Mg^{+2} and DNA concentrations. In systems where additional energy is supplied and where a fuel source is absent, the trade-off is absent, suggesting the trade-off arises from limitations in the regulation of translation and efficient energy regeneration. This work represents a significant advancement in understanding the effects of fuel and energy metabolism on TX-TL in cell-free systems and lays the foundation for improving TX-TL performance, lifetime, standardization, and prediction.

2 Results

2.1 Titration of TX-TL components in the absence of 3-PGA sheds light on the pairwise interactions of 3-PGA and these components

In order to gain more insight into the metabolism of energy and fuel in the TX-TL system, the effects of individual components of the system remained to be determined. Previous work, done in this group and others, has attempted to modulate these components indirectly – such as by performing TX-TL in a continuous, dialysis environment rather than a batch condition – or directly [1, 4]. The latter efforts have mostly employed a Design-of-Experiments approach, where some of the roughly 38 components of a TX-TL reaction are varied at random concentrations and the effects on protein expression are observed. A study by Borkowski and co-workers went one step further and used an active learning approach, where early and successive rounds of combinatorial screening were followed by learning, to inform the combinations of TX-TL component concentrations to use for subsequent iterations [4]. However, as these studies were exploratory rather than hypothesis-driven, only a small fraction of the large sample space was surveyed. Thus, while the qualitative effects

of several TX-TL components, either individually or through interactions with other components, have been identified, neither the mechanisms of their effects of TX-TL nor methods of modeling these interactions have been identified. As Poole's model of metabolism implied that (1) adding more or less fuel than the optimal amount should result in lower protein expression, (2) adding waste at the beginning of a reaction should inhibit TX-TL, and (3) adding more energy may improve TX-TL yields, these claims remained to be validated experimentally.

In initial experiments, TX-TL reactions were implemented with all components fixed (relative to a "standard" TX-TL composition [28]) except for the components of interest: 3-PGA, the fuel used to drive energy regeneration; NTPs, the molecules providing energy for TX-TL; candidate waste molecule inorganic phosphate (P_i); Mg^{+2}, whose chelation by P_i is a proposed mechanism for limited TX-TL lifetime, and whose addition should improve endpoint protein yields; and NAD^+, another energy molecule. These molecules were added at 0%, 25%, 50%, 150%, or 200% of their baseline values. While preliminary results didn't reveal anything unexpected (see Supplementary Information, Section A.4, for full results and analysis), the data suggested that adding more 3-PGA or less Mg^{+2} slightly increased protein yields. This contradicted previous findings that had found 30mM 3-PGA to be the optimal concentration for TX-TL [28] well as the results of a Mg^{+2} panel that had optimized Mg^{+2} concentration for this batch of cell lysate (**AR_ZJ** lysate; see Fig. A.1).

These early results raised many more questions: to what extent is 3-PGA used for energy regeneration versus waste accumulation? Similarly, what is the interaction (either direct or indirect) between 3-PGA and other TX-TL components? To answer these questions, the next set of experiments were similar to those performed in Section A.4, albeit with the exclusion of NAD^+ and GTP titrations, since the former seemed to have no effect on final TX-TL yields or dynamics (data not shown) and since the latter was not directly regenerated by fuel sources. Protein expression dynamics for these experiments are shown below (Fig. 1).

The data show that TX-TL is not possible in the absence of both 3-PGA and NTPs, but that TX-TL is possible in the absence of ATP, suggesting that (1) 3-PGA plays a key role in NTP regeneration, as expected, (2) one or more proteins or pathways (e.g. Nucleoside diphosphate kinase) are indeed active in converting other NTPs to ATP, and (3) in the absence of energy regeneration, adding more NTPs to the system may help recover lost function. Adding roughly 3mM ATP (i.e. doubling ATP compared to the standard concentration of 1.5mM) was not sufficient

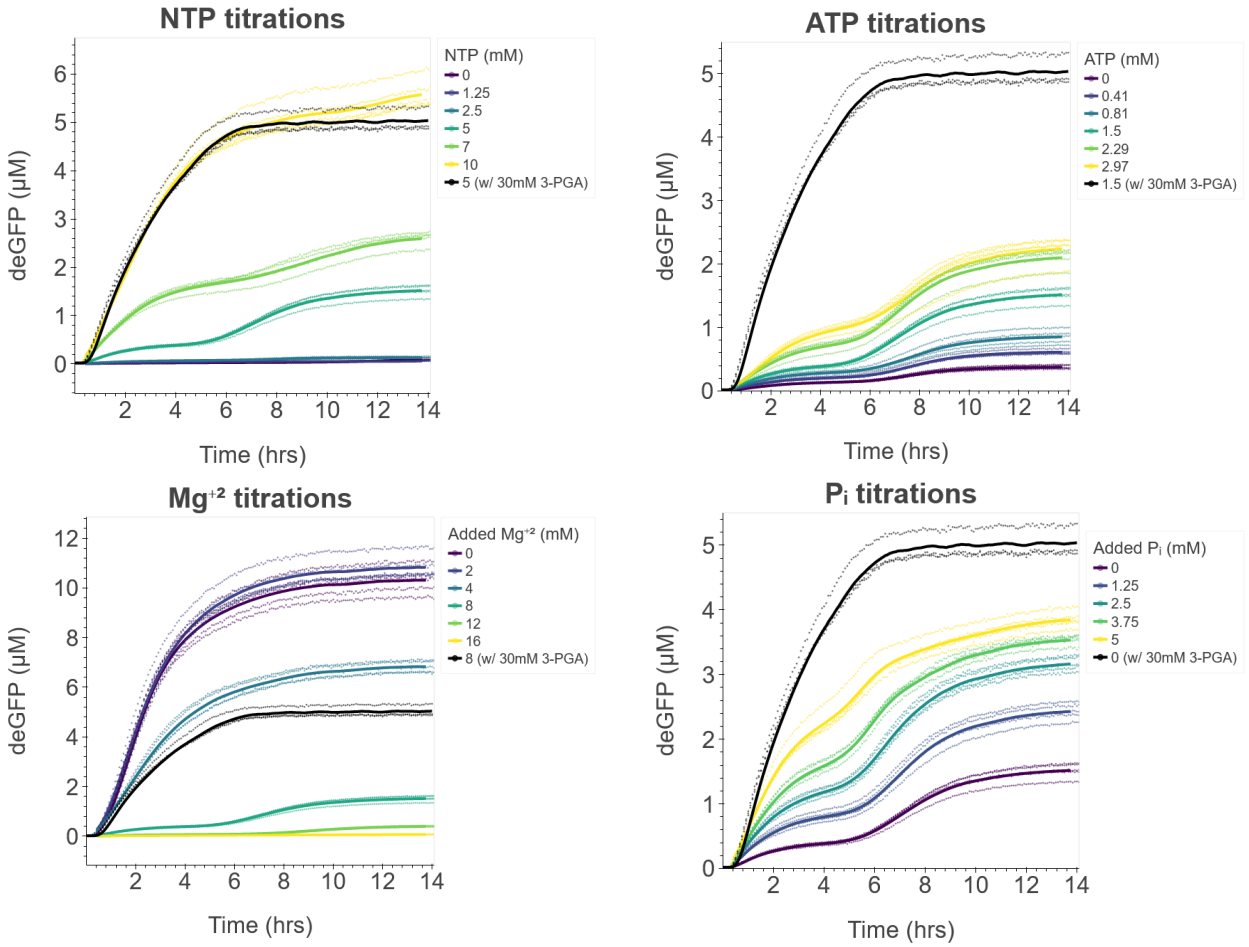

Figure 1: deGFP time-course measurements after titration of TX-TL reaction components in the absence of 3-PGA. Positive control standard (i.e. comparison with the addition of the standard 30mM 3-PGA) is shown as a black line in each plot. For these experiments, the **AR_ZJ** lysate was used with 2.4nM template DNA coding for deGFP. Average of 3 replicates (for positive control) or 5 replicates (for all other samples) is shown as a solid line; all data overlaid as points.

for recovering this lost function, perhaps because a fuel-less TX-TL system is energy-limited and can only make a lower amount of deGFP before rapid waste accumulation or energy dissipation.

The data also showed a very peculiar phenomenon; in the absence of 3-PGA, both lower concentrations of added Mg^{+2} (relative to the optimal concentration determined by the salt calibration) or any added amount of P_i improved both the maximum rate of protein production as well as the endpoint deGFP yields acquired. In the case of 0-2mM added Mg^{+2}, protein expression was approximately doubled. The fact that increased protein expression could be achieved with the addition of P_i, which chelates Mg^{+2} and removes it from the TX-TL system via precipitation, supported the idea that in the absence of 3-PGA, less Mg^{+2} is beneficial for TX-TL.

2.2 Mg^{+2} vs. 3-PGA panels suggest a trade-off between TX and TL

Initial experiments had suggested that optimal TX-TL occurred at increasing concentrations of Mg^{+2} for increasing concentrations of 3-PGA, For this set of experiments, two different batches of cell lysate were used: (1) **AR_ZJ** lysate, where cells where lysed using sonication, and (2) **DAJ_MK_MY** lysate, where cells were lysed using a French cell press and the cell lysate was dialyzed in later steps (see Methods section for more details). Two different DNA concentrations, 1nM and 5nM, were used in the experiments using **AR_ZJ** lysate, while 5nM DNA was used in the experiments using **DAJ_MK_MY** lysate. The endpoint deGFP yields obtained from these experiments is shown below (Fig. 2).

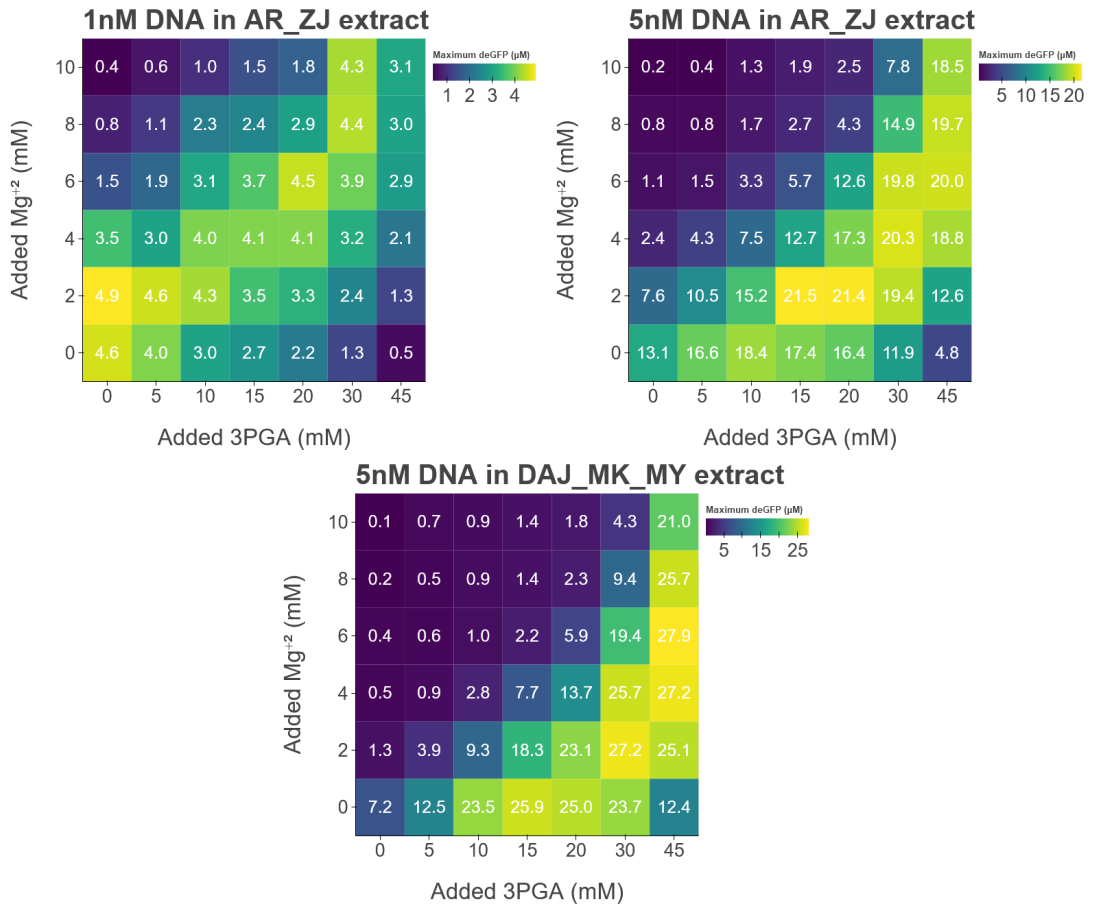

Figure 2: Endpoint deGFP measurements for three different Mg^{+2} vs. 3-PGA screens. From top left to bottom, three different experimental conditions were used: (1) **AR_ZJ** lysate with 1nM DNA, (2) **AR_ZJ** lysate with 5nM DNA, and (3) **DAJ_MK_MY** lysate with 5nM DNA. For reference, standard TX-TL formulations use 30mM 3-PGA and 4-10mM Mg^{+2}, with the latter depending on the results of a Mg^{+2} vs. K^{+} salt screen for a given batch of cell lysate. Three biological replicates were used for each experimental condition, and the mean fluorescence value of each condition is in the panels above. Colorbars are scaled separately for each plot.

The data confirm the finding that high endpoint deGFP measurements are found where increasing 3-PGA concentrations are associated with increasing Mg^{+2} concentrations. Even TX-TL reactions with 3-PGA concentrations as low as 10mM can achieve 80% of the maximum possible deGFP yields observed at higher concentrations of 3-PGA, supporting the possible hypotheses that (1) a significant amount of the energy regeneration potential of 3-PGA is being wasted, particularly at higher concentrations of Mg^{+2}, and/or (2) that 3-PGA metabolism is regenerating energy faster than it can be effectively utilized by the TX-TL system.

Previous studies have found that metabolism of 3-PGA and other fuel sources to pyruvate generates inorganic phosphate (P_i) as a byproduct of ATP regeneration [35], and that this P_i chelates Mg^{+2} [18], which is an important ion with roles in DNA and mRNA stability, enzyme function and allostery, and bioavailability of ATP. It is worth noting that the extent of Mg^{+2} binding is very high *in vivo*; in *E. coli*, of the 20-100mM of total Mg^{+2}, only 1-2mM is free, while the rest is bound to enzymes and nucleic acids [31]. In the experimental data shown here, however, it was not clear whether the additional Mg^{+2} was compensating for the additional P_i generated via metabolism of additional 3-PGA, or whether additional 3-PGA was compensating for energy dissipation accelerated by more Mg^{+2} in the form of Mg-ATP. It is possible that both hypotheses are true, as they are not mutually exclusive.

The data also show that optimal pairwise concentrations of Mg^{+2} and 3-PGA shift towards lower Mg^{+2} at higher concentrations of DNA. A hypothesis for this is that lower concentrations of DNA, more Mg^{+2} may be necessary to increase the rate of TX-TL and stabilize mRNA before waste rapidly accumulates and inhibits deGFP production, while at higher concentrations of DNA, the system is not mRNA-limited, so lower Mg^{+2} may be preferred to prevent Mg^{+2}-mediated waste accumulation or energy dissipation.

To determine whether Mg^{+2}-mediated regulation of TX-TL was acting at the level of transcription, translation, or both, the *deGFP* mRNA transcript was tagged with a Malachite Green aptamer (MGaptamer) sequence for *in vitro* labelling and live measurements over the course of a TX-TL experiment. Mg^{+2} versus 3-PGA panels for integrated mRNA measurements were plotted, the results of which are shown below (Fig. 3).

While MGaptamer measurements were at the limit of detection for the experiments where 1nM DNA was used, resulting in inconclusive data, in the experiments where 5nM DNA was used,

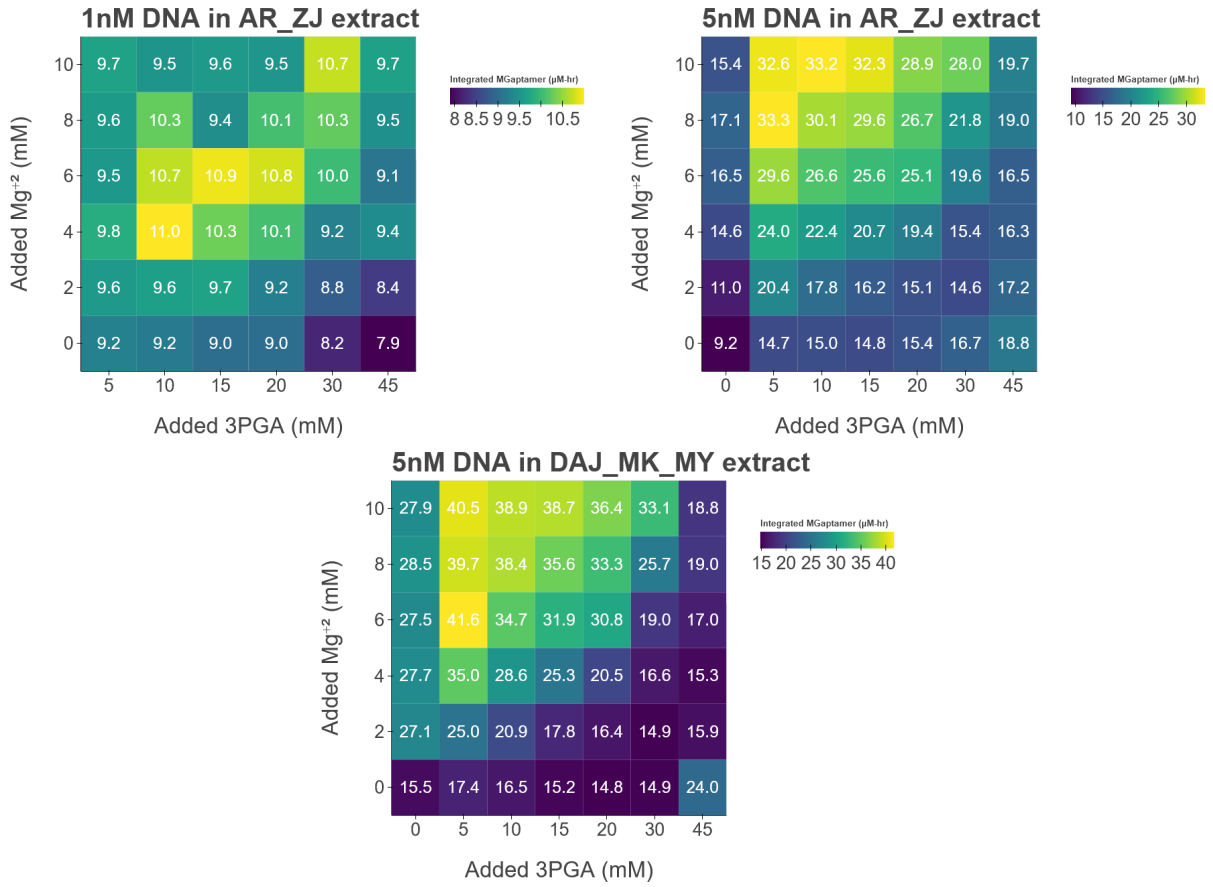

Figure 3: Integrated mRNA measurements for three different Mg^{+2} vs. 3-PGA screens. From top left to bottom, three different experimental conditions were used: (1) **AR_ZJ** lysate with 1nM DNA, (2) **AR_ZJ** lysate with 5nM DNA, and (3) **DAJ_MK_MY** lysate with 5nM DNA. For reference, standard TX-TL formulations use 30mM 3-PGA and 4-10mM Mg^{+2}, with the latter depending on the results of a Mg^{+2} vs. K^{+} salt screen for a given batch of cell lysate. Three biological replicates were used for each experimental condition. Colorbars are scaled separately for each plot.

maximum transcription occurred in the regime of high Mg^{+2} and low 3-PGA. Optimal transcription conditions appeared to be where translation was poor, and vice versa. This raised a major question: what was the cause of the observed phenomenon? It was possible that different Mg^{+2} and 3-PGA concentrations were simply optimal for transcription versus translation, but the phenomenon could also be due to inhibition of translation by transcription or vice versa. There also remained the possibility that either transcription or translation preferred a particular Mg^{+2} and 3-PGA regime, and that the other process was optimal where more resources were available for it.

2.3 Decoupling of transcription and translation suggests the observed trade-off is in part due to regulation of translation

To gain insight into the experimentally observed phenomenon, transcription and translation were decoupled. To perform a transcription-only reaction, 200μg/mL tetracycline was added to the reaction mixture to inhibit translation initiation by binding to the 30S subunit of the ribosome [2], while for a translation-only system, purified mRNA was added instead of DNA (see Methods for more details). The results of these experiments are shown below (Fig. 4).

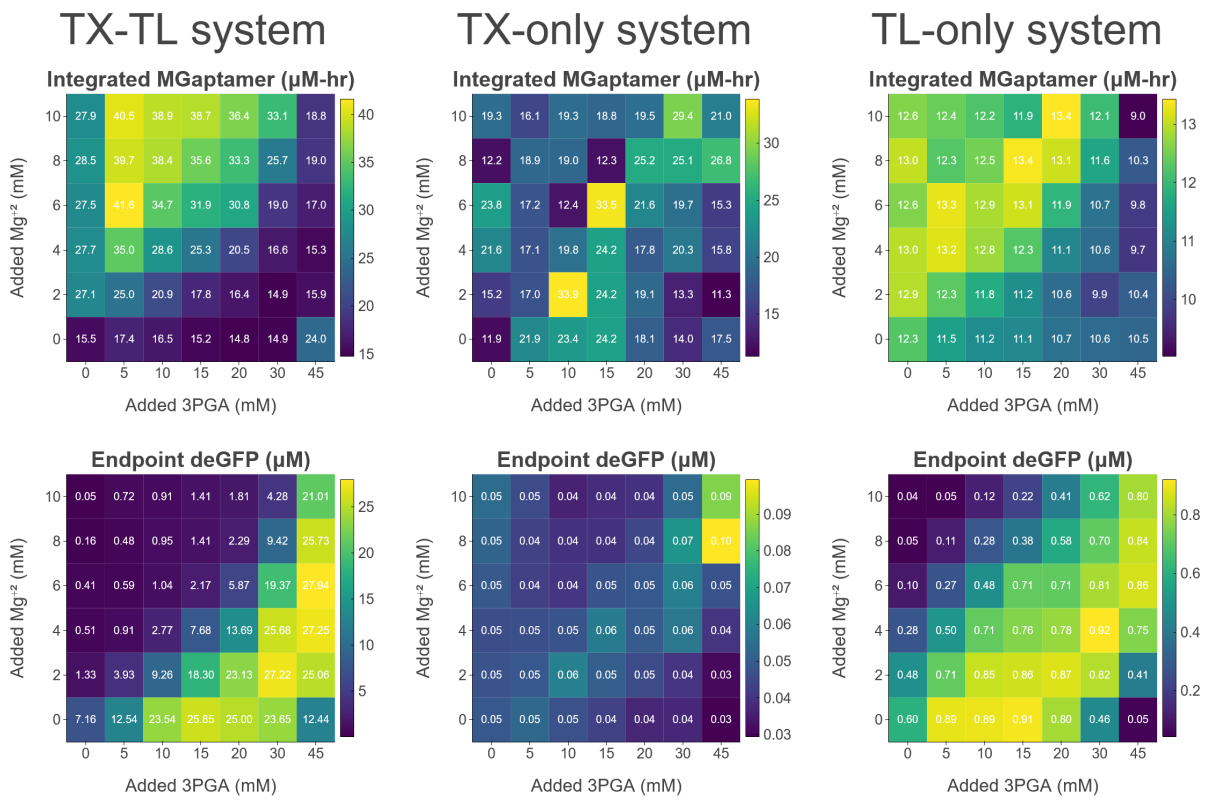

Figure 4: Decoupling of transcription (TX) and translation (TL). The left panel shows the coupled TX-TL system. The middle panel shows the TX-only system, to which 200μg/mL tetracycline has been added to inhibit translation. The right panel shows the TL-only system, where 0.3μM mRNA was added at the beginning of the reaction. The top plots are integrated mRNA measurements, and the bottom plots are endpoint deGFP measurements. All reactions shown use the **DAJ_MK_MY** lysate, and the TX-TL and TX-only systems use 5nM DNA. For reference, standard TX-TL formulations use 30mM 3-PGA and 4-10mM Mg^{+2}, with the latter depending on the results of a Mg^{+2} vs. K^{+} salt screen for a given batch of cell lysate. Three biological replicates were used for each experimental condition. Colorbars are scaled separately for each plot.

In the TX-only system, MGaptamer expression was not optimized at any particular regime of Mg^{+2} or 3-PGA. Meanwhile, in the TL-only system, higher endpoint deGFP yields were achieved as

before, at lower Mg^{+2} and higher 3-PGA concentrations, despite the mRNA persisting for longer at higher Mg^{+2} and lower 3-PGA concentrations. Control experiments indicated that the fluorescence of deGFP was not affected by the reaction conditions, and that MGaptamer and deGFP fluorescence are not strongly dependent on pH, Mg^{+2}, or 3-PGA for the reaction conditions considered in this work (see Supplementary Information, Fig. A.3 and Fig. A.4).

These data suggest that the previously observed TX-TL trade-off is, in part, due to translation being optimized at lower Mg^{+2} and higher 3-PGA concentrations, increased MGaptamer stability at higher Mg^{+2} and lower 3-PGA concentrations, and resource allocation in the TX-TL system (i.e. transcription is optimal where there are more resources available for it, specifically conditions where translation is not optimal). While these experiments did not shed light on the mechanism governing translation optimization at lower Mg^{+2} and higher 3-PGA concentrations, they further supported the hypothesis that there is a trade-off between transcription and translation in the cell-free systems used in this study.

2.4 A universal trade-off between transcription and translation

Regarding the trade-off between transcription and translation, another question also remained: was this phenomenon unique to systems where 3-PGA was used to regenerate energy, or did it also hold for other fuels that could be used to regenerate energy? Answering this question could help shed light on whether the observed phenomenon was caused by the metabolism of 3-PGA. To answer this question, the Mg^{+2} versus Fuel panels were repeated for three alternative fuels relevant to *E. coli* core metabolism: pyruvate, maltose, and succinate.

Pyruvate is located downstream of 3-PGA in the Glycolysis pathway and can participate in energy regeneration albeit without contributing potential waste molecule inorganic phosphate (P_i) to the system. Maltose, which consumes P_i and outputs a glucose molecule and glucose-6-phosphate (G6P) molecule, has been used previously to improve energy regeneration by recycling P_i [10]. However, as one maltose molecule can be used to generate two G6P molecules, and thus four 3-PGA molecules, maltose produces more acetate, ethanol, lactate and formate (additional candidate waste molecules) per molar compared to the other three fuels. Finally, succinate was also considered, since the addition of succinate should slow down/prevent GTP regeneration by succinyl-CoA, thus reducing the overall rate of energy regeneration. The assumption made here was that TX-TL

reactions have greater rates of energy consumption than other metabolic processes, but that when TX-TL resources (e.g. ribosomes, RNA polymerase, etc.) are loaded, much of the energy regenerated by the fuel source is wasted. Using succinate as a fuel source may slow down the rate of energy regeneration to a level where energy is used more efficiently by TX-TL.

The results of these screens are located in the Supplementary Information (Fig. A.7, A.8, A.9). While using alternative fuel sources did not replicate the linear trend for deGFP expression observed in the case of 3-PGA (Fig. 2), the experiments revealed some relevant results. First, they confirmed that the pairwise concentrations of Mg^{+2} and fuel that yielded high deGFP yields were mutually exclusive with those that yielded high integrated MGaptamer. Second, they showed that TX-TL was possible even when using non-phosphorylated fuel sources, and that the deGFP yields achieved were often as high as 50-75% of the yields achieved when using 3-PGA, for a given batch of cell lysate and DNA concentration. Finally, the screens suggested that there was not a single optimal Mg^{+2} concentration across the various fuel sources; while lower concentrations tended to yield the highest endpoint deGFP yields, optimal Mg^{+2} and fuel concentrations were unique to a batch of lysate, a concentration of DNA, and the fuel molecule used. Overall, these results suggested that while different fuels had different fuel regeneration and waste accumulation capabilities, there was indeed a universal trade-off between transcription and translation.

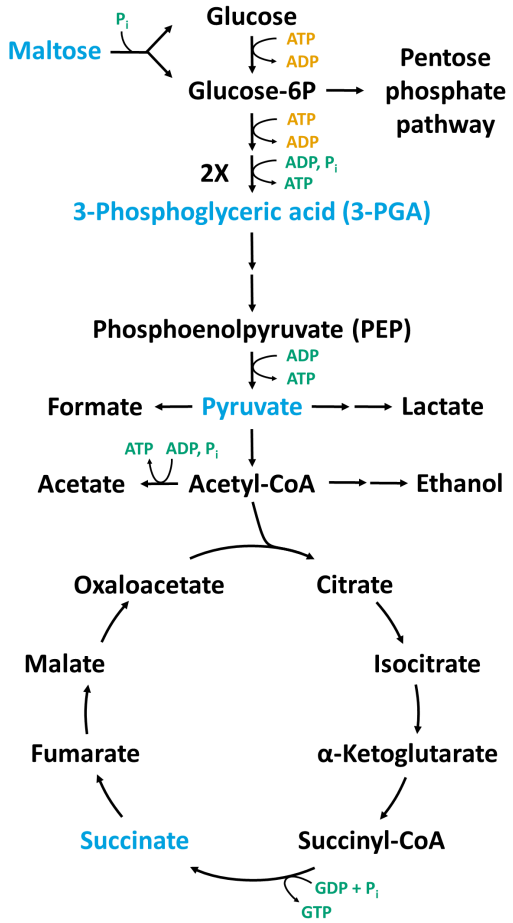

Figure 5: Simplified map of *E. coli* core metabolism with NTP consumption and regeneration. A simplified glycolysis, TCA cycle, and interacting branch of the Pentose Phosphate Pathway are shown. Metabolites used as a main fuel source for energy regeneration in the experimental work described here are indicated in **blue**. NTP consumption is indicated in **orange**, while NTP regeneration is indicated in **green**. Consumption/regeneration of other co-factors – such as NADH, FADH, QH_2, H_2O, and CO_2 – is omitted for simplicity.

2.5 The universal trade-off between transcription and translation is controlled by Mg^{+2} concentration

Overlaying the results of the Mg^{+2} versus Fuel panels for all the different experimental conditions confirmed that there was indeed a universal trade-off between transcription and translation (Fig. 6), and that Mg^{+2} (Fig. 6(a)) and DNA concentration (Fig. 6(b)) largely determined where a particular experimental system lay along the trade-off curve.

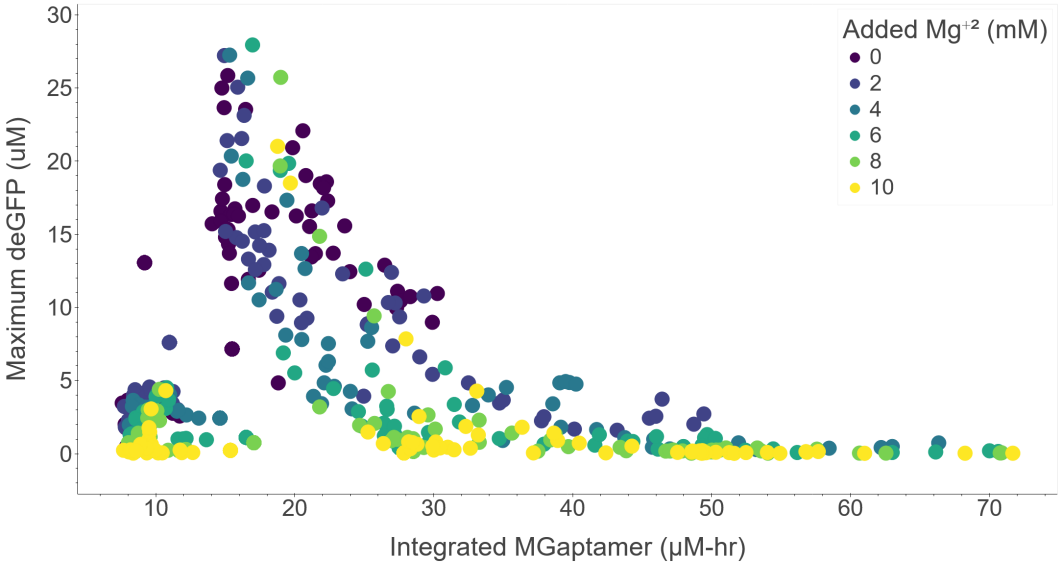

(a) Points colored by Mg^{+2} concentration

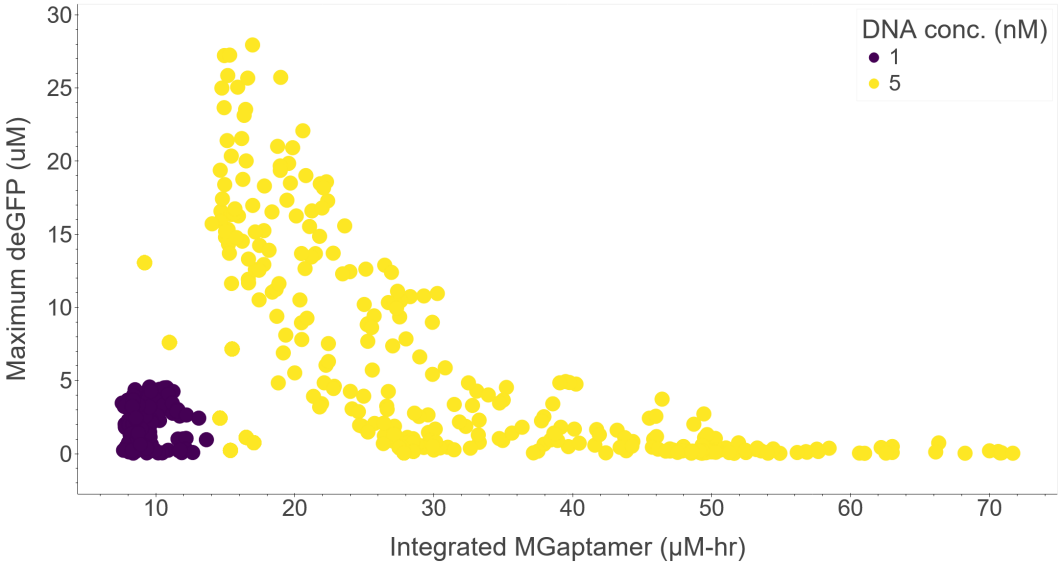

(b) Points colored by DNA concentration

Figure 6: Endpoint deGFP concentrations versus integrated MGaptamer fluorescence. Each point represents an individual sample.

Specifically, DNA concentration shifted the trade-off curve towards greater integrated MG aptamer, while Mg^{+2} concentration determined where a system lay along the curve corresponding to a particular DNA concentration, with lower Mg^{+2} correlated with higher deGFP endpoint concentrations and vice versa.

Fuel type had some effect on where a particular experimental system lay along the trade-off curve, while fuel concentration did not (see Supplementary Information, Fig. A.10). Interestingly, points that did not fall along the trade-off curves were all data from TX-TL reactions to which no fuel had been added (Fig. A.10). To some extent, the variability among points along the trade-off curve could be explained by the batch of cell lysate used for a given experiment (see Supplementary Information, Fig. A.11).

As the different fuels have different impacts on energy metabolism, separate plots were also made for the individual fuel sources, where again the location of points on the plot could be determined by, in order of increasing impact, cell lysate, DNA concentration, and Mg^{+2} concentration (see Supplementary Information, Fig. A.12).

2.6 The TX-TL trade-off is absent when TX-TL systems are supplied with no fuel and additional energy

Regarding the question of whether TX inhibited TL or whether conditions that favored TX-TL were mutually exclusive, experiments in which no fuel was used – but the concentration of NTPs was modified – offer an insight. The results of these experiments suggest that the previously observed trade-off is only present when using the fuels participating in core metabolism – 3-PGA, pyruvate, succinate, and maltose – and not in the absence of these fuels (Fig. 7). When using NTPs as a fuel (i.e. using a greater concentration of NTPs to compensate for the lack of energy regeneration by an added fuel source), high values of integrated MGaptamer were achieved without corresponding decreases in endpoint deGFP yields, except at exceptionally high concentrations of MGaptamer. These data seem to suggest that the TX-TL trade-off indeed rises, in part, from a limitation in energy metabolism.

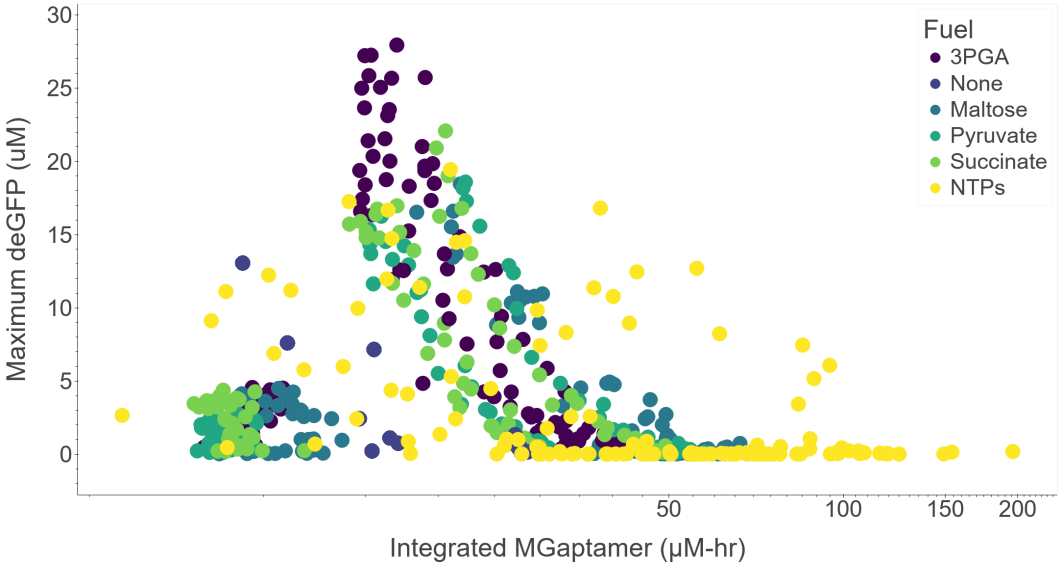

Figure 7: Endpoint deGFP concentrations versus integrated MGaptamer fluorescence, with additional data from experiments where NTP concentrations were varied. Points are colored by fuel type, and a log-axis is used for the integrated MGaptamer axis. Each point represents an individual sample.

3 Discussion

An improved understanding of cell-free metabolism is essential to gaining a greater qualitative and quantitative understanding of cell-free TX-TL. The experimental results shown here have contributed to this effort by discovering and characterizing a trade-off between transcription and translation in an *E. coli*-based cell-free TX-TL system. This work has shown that the trade-off arises from regulation of translation in the 3-PGA-fueled system, and that the trade-off is not only universal across the four central carbon fuels used in this study – 3-PGA, pyruvate, maltose, and succinate – but also that it is mediated strongly by Mg^{+2} and DNA concentrations. Finally, this study showed the trade-off is absent in systems with additional NTPs and no fuel. Taken together, these data have strong implications for understanding the effects of fuel and energy metabolism in cell-free TX-TL system.

These findings suggest that the observed trade-off between transcription and translation may reflect a trade-off between rapid energy regeneration and efficient energy consumption and/or waste accumulation. Under this hypothesis, when Mg^{+2} is low, energy regeneration is low enough that energy is more efficiently used by TX-TL and less energy goes towards other metabolic processes. But when Mg^{+2} is high, energy is regenerated more rapidly, albeit at a rate higher than can be

utilized by TX-TL resources, so the excess energy is used by metabolic processes that metabolize fuel into inert products or waste products harmful to TX-TL. This hypothesis is supported by the following:

- a previous finding that there is an NTP- and Mg^{+2}-dependent suppression of TX-TL [20]
- the fact that maltose has a greater energy regeneration and waste accumulation capacity (per molar concentration) than the other fuels, and that points corresponding to maltose as a fuel source lie lower on the trade-off curve (towards the conditions that favor waste accumulation; Fig. A.10)
- experimental data showing high deGFP endpoint yields achieved across a broad range of integrated MGaptamer values only when NTPs are used as a fuel, suggesting that metabolism of the fuels in the presence of high NTP concentrations, rather than high NTP concentrations alone, is contributing to TL inhibition

It appears that only TL is inhibited by Mg^{+2}-mediated metabolic changes, while TX processes are able to utilize available energy for increased MGaptamer expression.

With regards to the energy trade-off, the data do not help explain whether poor translation is caused by energy too rapidly regenerated to be used by translation (e.g. in a ribosome-limited system) or by the accumulation of waste due to the metabolism of central carbon fuels. In the experiments where no central carbon fuel was used, and higher concentrations of NTPs were used to compensate for the lack of energy regeneration, the concentration of Mg^{+2} used was only 0-2mM, so there is not enough evidence to support one hypothesis or the other (or both). If the waste accumulation hypothesis is true, the fact that the TX-TL trade-off exists even in the absence of a phosphorylated fuel source suggests inorganic phosphate is not the cause of limited TX-TL lifetime, as is often suggested by existing literature. Rather, the accumulation of some currently unidentified waste product is causing this limited lifetime. As data from experiments using NTPs as a fuel source did not lie along the trade-off curve, it appears that a bulk of cell-free metabolic waste is generated by *E. coli* core metabolism. Furthermore, the presence of high deGFP yields at high values of integrated MGaptamter values, where high concentrations of NTPs were added to the beginning of a TX-TL reaction, also rules out the possibility that transcriptional waste alone

is inhibiting translation. To further investigate energy metabolism, dynamic NTP measurements of TX-TL systems at different points along the trade-off will be necessary, and they are a future goal of this work.

Although it is not clear exactly how Mg^{+2} is modulating a TX-TL system's position along the trade-off curve, possible hypotheses that could explain this phenomenon are (1) increased Mg^{+2} may make NTPs more available for metabolic processes, since NTPs are commonly bioavailable only as Mg-NTP; (2) Mg^{+2} concentration may be modulating optimal ribosome activity; and/or (3) higher Mg^{+2} may be increasing the activity of enzymes that generate waste that inhibits translation. Experiments where concentrations of ATP and GTP were modulated separately suggest that additional GTP improves endpoint deGFP yields more so than additional ATP (Fig. A.6), which is important in light of the fact that GTP is used more heavily in translation compared to ATP. In addition to NTP measurements, experiments investigating ribosome activity are an additional future direction of this work, to gain a deeper understanding of translation regulation in the TX-TL system.

In light of these insights, how might an improved understanding of cell-free metabolism be used to improve TX-TL performance (e.g. increase the rate of TX-TL, protein yields, etc.)? Additionally, regardless of whether improvement of TX-TL is possible, how might this new knowledge aid computational modelling efforts aimed at predicting TX-TL? Regarding the former, the data shown here suggest that if there is a way to perform energy regeneration without generating waste that may inhibit TX-TL, then improving TX-TL performance may be possible. Regarding improved prediction of TX-TL, by showing that Mg^{+2} concentration can explain much of the variability across different TX-TL systems, this experimental work has informed an updated cell-free metabolism model that may be able to accurately predict TX-TL dynamics better than existing models (Fig. 8). Future efforts aimed at performing Bayesian parameter inference for phenomenological models of TX-TL systems should help with efforts aimed at prediction of cell-free TX-TL performance. If these efforts are successful, this modeling framework could also be used with an existing model-based calibration methodology to standardize performance across cell-free systems [27].

While this work represents a significant advancement in the understanding of cell-free metabolism, future work will validate and characterize the aforementioned hypotheses as well as to utilize these findings in applications relevant to cell-free synthetic biology.

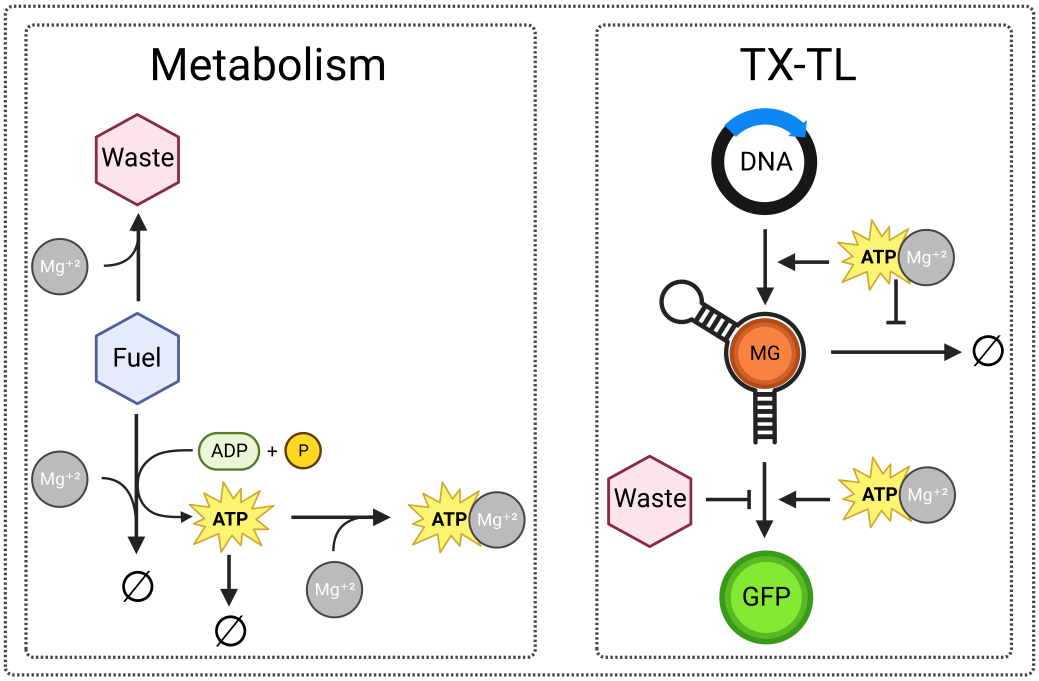

Figure 8: An updated phenomenological model of cell-free TX-TL coupled to metabolism. This model includes a role for Mg^{+2}.

4 Methods

4.1 Preparation of cell lysate

Cell lysate was prepared from *E. coli* BL21 Rosetta2 cells using the protocol established by Sun and co-workers [28] with some modifications. Briefly, cells were grown sequentially in 6mL, 100mL, and 1L cultures, where smaller cultures were used to inoculate larger ones. Once 6L of culture had grown to roughly an OD600 of 2, cells were repeatedly centrifuged and washed with S30B buffer by re-suspension. Cells were then re-suspended in S30B buffer and subjected to cell lysis.

For the DAJ_MK_MY lysate, cells were re-suspended at 1.4g cells per mL of S30B buffer and lysed by a French cell press at a pressure of 640psi. For the AR_ZJ lysate, cells were re-suspended to 1g cells per mL of S30B buffer and lysed by sonication at a probe frequency of 20 kHz and an amplitude of 50%. Cells were sonicated at 10-second ON/OFF intervals for a total of 60 seconds ON (6 ON/OFF cycles), resulting in approximately 300 Joules of energy delivered. After both methods of cell lysis, 3μL of DTT was added per mL of cell lysate, and the lysates were then centrifuged to remove cell debris.

Both batches of lysate were then subjected to a 1-hour run-off reaction at 37°C, after which they were subjected to centrifugation to remove additional debris. The DAJ_MK_MY lysate was subjected to dialysis in S30B buffer for four hours. Finally, both batches of cell lysate were aliquoted, flash-frozen in liquid nitrogen, and stored at -80°C until further use.

4.2 Plasmid sequence used to express deGFP

The plasmid used to express deGFP was prepared by Dan Siegal-Gaskins and modified by Zoila Jurado Quiroga to change the T7 promoter to a pOR1OR2 promoter. The plasmid is pOR1OR2-MGaptamer-UTR1-deGFP-T500. The following is the sequence of the plasmid.

TGAGCTAACACCGTGCGTGTTGACAATTTTACCTCTGGCGGTGATAATGGTTGCAGCTAGCGGGATCCCGACTGGCGAGAGC
CAGGTAACGAATGGATCCAATAATTTTGTTTAACTTTAAGAAGGAGATATACCATGGAGCTTTTCACTGGCGTTGTTCCCAT
CCTGGTCGAGCTGGACGGCGACGTAAACGGCCACAAGTTCAGCGTGTCCGGCGAGGGCGAGGGCGATGCCACCTACGGCAAG
CTGACCCTGAAGTTCATCTGCACCACCGGCAAGCTGCCCGTGCCCTGGCCCACCCTCGTGACCACCCTGACCTACGGCGTGC
AGTGCTTCAGCCGCTACCCCGACCACATGAAGCAGCACGACTTCTTCAAGTCCGCCATGCCCGAAGGCTACGTCCAGGAGCG
CACCATCTTCTTCAAGGACGACGGCAACTACAAGACCCGCGCCGAGGTGAAGTTCGAGGGCGACACCCTGGTGAACCGCATC
GAGCTGAAGGGCATCGACTTCAAGGAGGACGGCAACATCCTGGGGCACAAGCTGGAGTACAACTACAACAGCCACAACGTCT
ATATCATGGCCGACAAGCAGAAGAACGGCATCAAGGTGAACTTCAAGATCCGCCACAACATCGAGGACGGCAGCGTGCAGCT
CGCCGACCACTACCAGCAGAACACCCCCATCGGCGACGGCCCCGTGCTGCTGCCCGACAACCACTACCTGAGCACCCAGTCC
GCCCTGAGCAAAGACCCCAACGAGAAGCGCGATCACATGGTCCTGCTGGAGTTCGTGACCGCCGCCGGGATCTAACTCGAGC
AAAGCCCGCCGAAAGGCGGGCTTTTCTGTGTCGACCGATGCCCTTGAGAGCCTTCAACCCAGTCAGCTCCTTCCGGTGGGCG
CGGGGCATGACTATCGTCGCCGCACTTATGACTGTCTTCTTTATCATGCAACTCGTAGGACAGGTGCCGGCAGCGCTCTTCC
GCTTCCTCGCTCACTGACTCGCTGCGCTCGGTCGTTCGGCTGCGGCGAGCGGTATCAGCTCACTCAAAGGCGGTAATACGGT
TATCCACAGAATCAGGGGATAACGCAGGAAAGAACATGTGAGCAAAAGGCCAGCAAAAGGCCAGGAACCGTAAAAAGGCCGC
GTTGCTGGCGTTTTTCCATAGGCTCCGCCCCCCTGACGAGCATCACAAAAATCGACGCTCAAGTCAGAGGTGGCGAAACCCG
ACAGGACTATAAAGATACCAGGCGTTTCCCCCTGGAAGCTCCCTCGTGCGCTCTCCTGTTCCGACCCTGCCGCTTACCGGAT
ACCTGTCCGCCTTTCTCCCTTCGGGAAGCGTGGCGCTTTCTCAATGCTCACGCTGTAGGTATCTCAGTTCGGTGTAGGTCGT
TCGCTCCAAGCTGGGCTGTGTGCACGAACCCCCCGTTCAGCCCGACCGCTGCGCCTTATCCGGTAACTATCGTCTTGAGTCC
AACCCGGTAAGACACGACTTATCGCCACTGGCAGCAGCCACTGGTAACAGGATTAGCAGAGCGAGGTATGTAGGCGGTGCTA
CAGAGTTCTTGAAGTGGTGGCCTAACTACGGCTACACTAGAAGGACAGTATTTGGTATCTGCGCTCTGCTGAAGCCAGTTAC
CTTCGGAAAAAGAGTTGGTAGCTCTTGATCCGGCAAACAAACCACCGCTGGTAGCGGTGGTTTTTTTGTTTGCAAGCAGCAG

ATTACGCGCAGAAAAAAAGGATCTCAAGAAGATCCTTTGATCTTTTCTACGGGGTCTGACGCTCAGTGGAACGAAAACTCAC
GTTAAGGGATTTTGGTCATGAGATTATCAAAAAGGATCTTCACCTAGATCCTTTTAAATTAAAAATGAAGTTTTAAATCAAT
CTAAAGTATATATGAGTAAACTTGGTCTGACAGTTACCAATGCTTAATCAGTGAGGCACCTATCTCAGCGATCTGTCTATTT
CGTTCATCCATAGTTGCCTGACTCCCCGTCGTGTAGATAACTACGATACGGGAGGGCTTACCATCTGGCCCCAGTGCTGCAA
TGATACCGCGAGACCCACGCTCACCGGCTCCAGATTTATCAGCAATAAACCAGCCAGCCGGAAGGGCCGAGCGCAGAAGTGG
TCCTGCAACTTTATCCGCCTCCATCCAGTCTATTAATTGTTGCCGGGAAGCTAGAGTAAGTAGTTCGCCAGTTAATAGTTTG
CGCAACGTTGTTGCCATTGCTACAGGCATCGTGGTGTCACGCTCGTCGTTTGGTATGGCTTCATTCAGCTCCGGTTCCCAAC
GATCAAGGCGAGTTACATGATCCCCCATGTTGTGCAAAAAAGCGGTTAGCTCCTTCGGTCCTCCGATCGTTGTCAGAAGTAA
GTTGGCCGCAGTGTTATCACTCATGGTTATGGCAGCACTGCATAATTCTCTTACTGTCATGCCATCCGTAAGATGCTTTTCT
GTGACTGGTGAGTACTCAACCAAGTCATTCTGAGAATAGTGTATGCGGCGACCGAGTTGCTCTTGCCCGGCGTCAATACGGG
ATAATACCGCGCCACATAGCAGAACTTTAAAAGTGCTCATCATTGGAAAACGTTCTTCGGGGCGAAAACTCTCAAGGATCTT
ACCGCTGTTGAGATCCAGTTCGATGTAACCCACTCGTGCACCCAACTGATCTTCAGCATCTTTTACTTTCACCAGCGTTTCT
GGGTGAGCAAAAACAGGAAGGCAAAATGCCGCAAAAAAGGGAATAAGGGCGACACGGAAATGTTGAATACTCATACTCTTCC
TTTTTCAATATTATTGAAGCATTTATCAGGGTTATTGTCTCATGAGCGGATACATATTTGAATGTATTTAGAAAAATAAACA
AATAGGGGTTCCGCGCACATTTCCCCGAAAAGTGCCACCTGACGTCTAAGAAACCATTATTATCATGACATTAACCTATAAA
AATAGGCGTATCACGAGGCCCTTTCGTCTTCAAGAATTCTGGCGAATCCTCTGACCAGCCAGAAAACGACCTTTCTGTGGTG
AAACCGGATGCTGCAATTCAGAGCGGCAGCAAGTGGGGGACAGCAGAAGACCTGACCGCCGCAGAGTGGATGTTTGACATGG
TGAAGACTATCGCACCATCAGCCAGAAAACCGAATTTTGCTGGGTGGGCTAACGATATCCGCGGATCCCGACTGATGCGTGA
ACGTGACGGACGTAACCACCGCGACATGTGTGTGCTGTTC

4.3 Preparation of template DNA plasmid

Template DNA for the cell-free reactions was prepared from *E. coli* KL740 cells (purchased from Arbor Biosciences) that had been transformed with the plasmid described above. Cells were grown overnight at 30°C and either Mini-prepped or Midi-prepped the next day using the appropriate protocols. When Mini-prepping, DNA was eluted with nuclease-free water; when Midi-prepping, after the concentration step, DNA was eluted with IDTE Buffer (10mM Tris-HCl, 0.1mM EDTA).

4.4 Preparation of cell-free reactions

Cell-free reactions were prepared as per the protocol by Sun and co-workers [28]. Unless otherwise noted, each reaction consisted of the following: 33% (by volume) of cell lysate, 1.5mM of each amino

acid (except for Leucine, which was added at 1.25mM), 1.5mM each of ATP and GTP, 0.9mM each of CTP and UTP, 50mM HEPES pH 8, 0.2mg/mL tRNA, 0.26mM Coenzyme A, 0.33mM NAD^+, 0.75mM cyclic AMP (cAMP), 0.068mM Folinic acid, 1mM Spermidine, 10μM Malachite Green Dye, and 30mM 3-PGA. Depending on the batch of cell lysate, a standard reaction used either 8mM magnesium glutamate and 80mM potassium glutamate (for the DAJ_MK_MY lysate) or 6mM magnesium glutamate and 140mM potassium glutamate (for the AR_ZJ lysate). For the Mg^{+2} versus Fuel panels, the 30mM 3-PGA and Mg^{+2} were omitted and replaced with the appropriate concentration of Mg^{+2} and 3-PGA or other fuel. Finally, depending on the experiments, a variable amount of DNA plasmid was added, and the remaining volume of the 10μL reaction was filled with nuclease-free water.

As reactions were all performed in 384-well glass-bottom plates, water, DNA, and components being titrated into the TX-TL reaction were added using the Echo 525 liquid handler, while the remaining components were added to a bulk solution and electronically dispensed by a multi-dispense pipette. To prevent the reaction from starting before all the components had been added in, all reagent were kept on ice until they were added to the reaction and added sequentially to reduce evaporation and/or degradation. First, a master mix minus the cell lysate was created and kept on ice in an Eppendorf tube; then, components to be added by Echo were added to the 384-well plate, where all stock concentrations were diluted to less than 500mM so that they could be effectively dispensed via Echo; next, the cell lysate was added to the master mix; finally, the master mix was pipetted to the wall of each well. Once the plate was covered with a plastic seal, it was centrifuged at 4000xg for 1 minute at 4°C. Finally, the bottom of the plate was quickly cleaned by Kimwipe to remove any debris and immediately transferred to a plate BioTek H1MF plate reader that had reached its setpoint of 30°C.

4.5 Dynamic measurements of MGaptamer and deGFP

Fluorescence measurements were performed by a BioTek H1MF plate reader at 30°C, and measurements were read from the bottom of the plate every 3 minutes (preceding by 5 seconds of linear shaking) at excitation/emission wavelengths suitable for MGaptamer (610/650nm, Gain 150) and deGFP (485/515nm, Gain 61). Arbitrary fluorescence units were converted to micromolar concentrations using a calibration curve prepared by purifying deGFP protein and MGaptamer mRNA

in-house and performing serial dilutions in PBS. The slope of the calibration curve was used to calibrate measurements (see Supplementary Information for calibration curves).

4.6 mRNA purification for a translation-only system

To obtain an mRNA sequence containing MGaptamer-UTR1-deGFP-T500, a linear DNA template was first prepared, followed by DNA isolation, *in vitro* transcription, DNAse treatment, and mRNA isolation. First, for generation of the linear DNA template, primers of the following sequences were first used to amplify the relevant sequence via a PCR reaction: CCAGAAAACC-GAATTTTGCTGG and ATGATAAAGAAGACAGTCATAAGTGCG. A 1-mL PCR reaction was performed using NEB Q5 2x Master Mix and run for 30 cycles with an elongation time of 45 seconds and an annealing temperature of 65°C.

After the PCR reaction was performed, the PCR was aliquoted to three 1.7-mL Eppendorf tubes (i.e. 333μL per tube) and DNA was precipitated by adding 33μL 3M sodium acetate and 1mL 100% ethanol per tube. After chilling the tubes at -80°C for 20 minutes, the tubes were centrifuged at 16000xg for 30 minutes at 4°C. Finally, all supernatant was pipetted out, and residual ethanol was allowed to evaporate by leaving the tubes open and uncovered at room temperature. The DNA was re-suspended in 50μL nuclease-free water per tube.

In vitro transcription was performed using the HiScribe®T7 High Yield RNA Synthesis Kit, and instructions included in the kit's manual were used for DNase I treatment of the reaction.

Finally, the synthesized mRNA was isolated using the PureLink RNA Mini kit. 100% ethanol was first added to the reaction to a final concentration of 35%, after which the kit's "Protocol for RNA clean-up and purification from liquid samples" was used (omitting the Lysis step). mRNA concentration was determined by a Nanodrop 2000c.

4.7 Translation inhibition using tetracycline

The translation inhibition experiments were performed in DAJ_MK_MY lysate by adding 200μg/mL to TX-TL reactions. Tetracycline solutions were created by dissolving tetracycline to 80mg/mL in DMSO, diluting the the solution to 5mg/mL in nuclease-free water, and dispensing the tetracycline using the Echo 525 liquid handler. To determine the optimal concentration of tetracycline to use for translation-inhibition, titrations were performed.

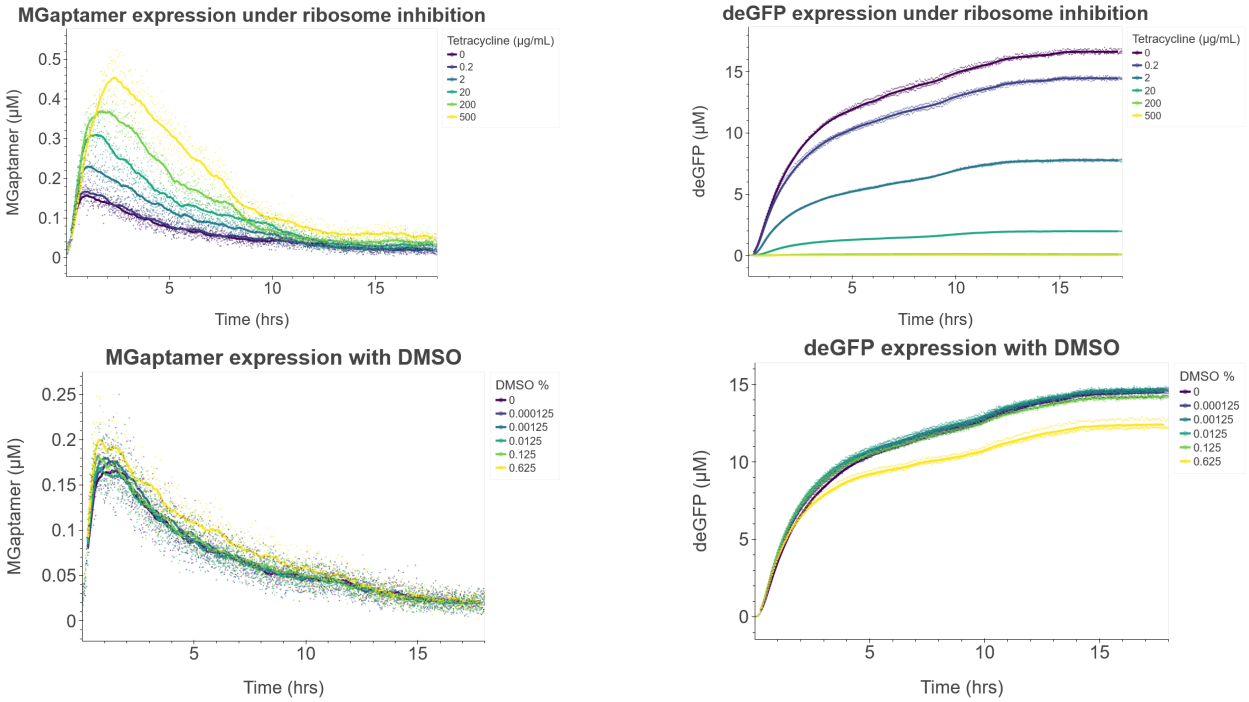

Figure 9: Titrations to determine concentration of tetracycline necessary for translation inhibition. Controls were performed by adding the equivalent amount of DMSO to make sure the tetracycline alone was impacting translation.

4.8 Data analysis

Fluorescence measurements of deGFP and MGaptamer were converted to micromolar concentrations via the calibration curves. Endpoint deGFP concentration was determined to be the maximum deGFP concentration achieved for a given experimental condition, averaged over three biological replicates. Integrated MGaptamer measurements were made by using the NumPy **trapz** package for numerical integration using the trapezoidal method, likewise averaged over three biological replicates.

5 Acknowledgements

The work described here would not be possible without the initial ideas that came out of extensive discussions with William Poole. While the primary goal of the initial collaboration was to generate data to validate his cell-free metabolism model, his suggestions to probe the roles of Mg^{+2} and different fuel sources helped generate new questions and analyses that led to the experiments discussed here. Apart from Poole, additional members of the lab – specifically Ankita Roychoudhury,

Zoila Jurado Quiroga, David Alexander Johnson, and Miryong (Miki) Yun – also contributed to the work shown here. Zoila was present in and contributed to many of these discussions with William, and all four helped prepared the cell lysate used in the experiments here. The authors thank Paul Freemont for his helpful comments over the past few months, particularly those pertaining to cell-free metabolism. Finally, ChatGPT was used to write part of the introduction section, which has been an interesting and helpful endeavor.

Research was sponsored by the Army Research Office and was accomplished under Cooperative Agreement Number W911NF-22-2-0210. The views and conclusions contained in this document are those of the authors and should not be interpreted as representing the official policies, either expressed or implied, of the Army Research Office or the U.S. Government. The U.S. Government is authorized to reproduce and distribute reprints for Government purposes notwithstanding any copyright notation herein.

6 Disclosures

RMM has a financial stake in Tierra Biosciences, a private company that makes use of cell-free technologies such as those described in this article for protein expression and screening. The other authors have nothing to disclose.

A Supplementary Information

A.1 Salt calibration of cell lysates

To determine the Mg^{+2} and K^{+} that would yield the maximum concentration of deGFP, salt panels were performed for each batch of cell lysate. Standard TX-TL reactions were prepared with 1nM DNA template plasmid to express deGFP. One biological replicate was used for each experimental condition. The optimal salt concentrations were then used for the appropriate cell lysates.

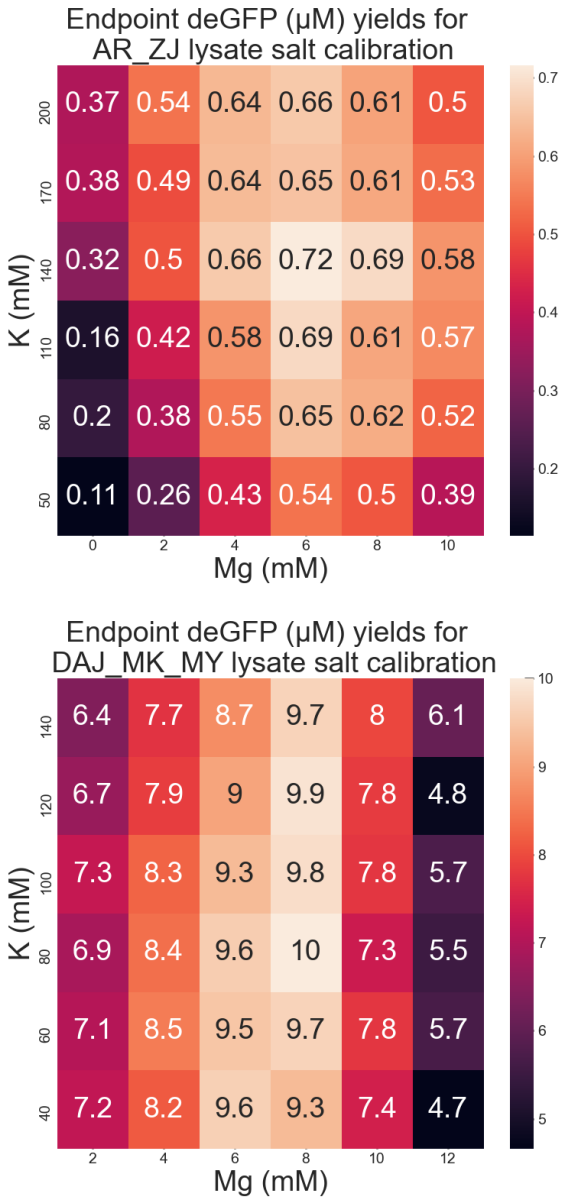

Figure A.1: Salt calibrations for cell lysates.

A.2 Calibration data for deGFP protein and MGaptamer mRNA

To create a deGFP fluorescence calibration curve, serial dilutions of eGFP (purchased from Cell Biolabs) were performed in 1X PBS, after which 3 x 10μL of each sample were loaded onto a 384-well plate and read by a BioTek H1MF plate reader at 30°C and at a Ex/Em wavelengths of 485/515 and a Gain of 61. 3 technical replicates were read over 3 minutes at 1-minute intervals to generate 4 points per replicate, and the average of these 12 points was used as a single point at a given concentration through which the calibration line was fit with a zero intercept.

To create a MGaptamer fluorescence calibration curve, mRNA of the MGaptamer sequence only – specifically `rArCrUrGrGrArUrCrCrCrGrArCrUrGrGrCrGrArGrArGrCrCrArGrGrUrArArCrGrArArU rGrGrArUrCrCrArArU` – was purchased from IDT DNA. The lyophilized mRNA was re-suspended in nuclease-free water at its concentration was determined by a Nanodrop 2000c. Next, serial dilutions of MGaptamer mRNA were performed in 1X PBS containing 10μM Malachite Green dye, after which 4 x 10μL of each sample were loaded onto a 384-well plate and read by a BioTek H1MF plate reader at 30°C and at a Ex/Em wavelengths of 610/650 and a Gain of 150. 4 technical replicates were read over 10 minutes at 2.5-minute intervals to generate 5 points per replicate, and the average of these 20 points was used as a single point at a given concentration through which the calibration line was fit with a zero intercept.

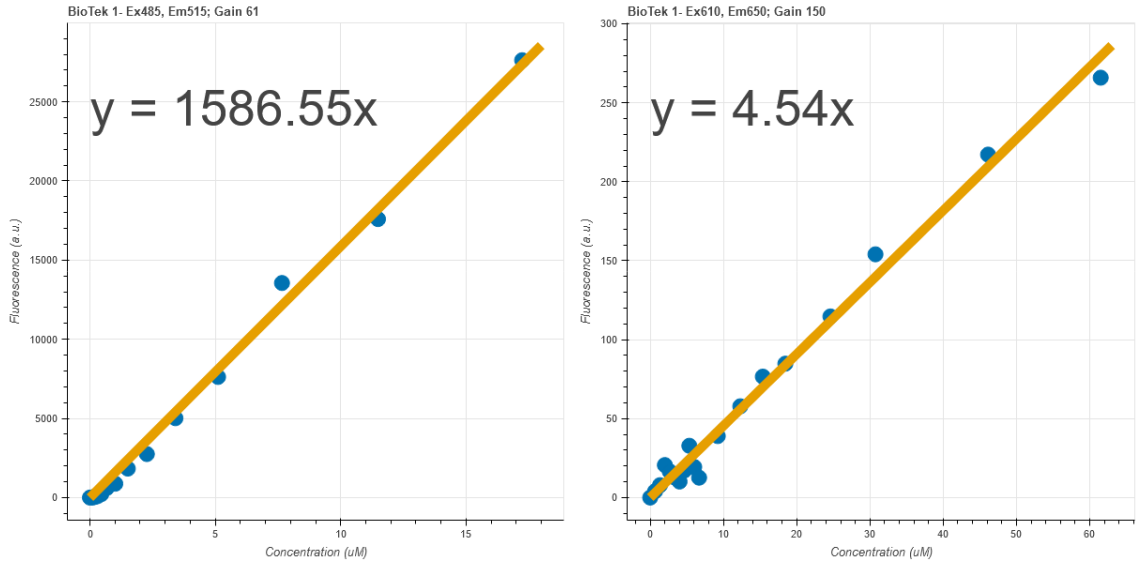

(a) eGFP calibration (b) MGaptamer calibration

Figure A.2: Fluorescence calibration curves

A.3 Exploring the dependence of MGaptamer and deGFP fluorescence on reaction conditions

To determine the extent to which MGaptamer and deGFP fluorescences, rather than expression, were affected by different reaction conditions, the effects of two different variables, pH and Mg^{+2} concentration, were explored.

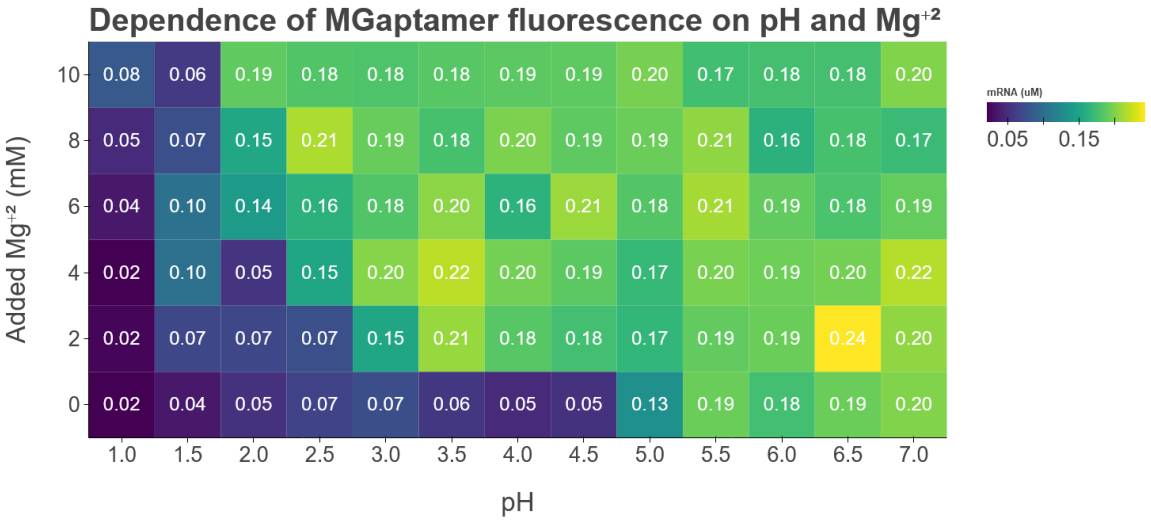

(a)

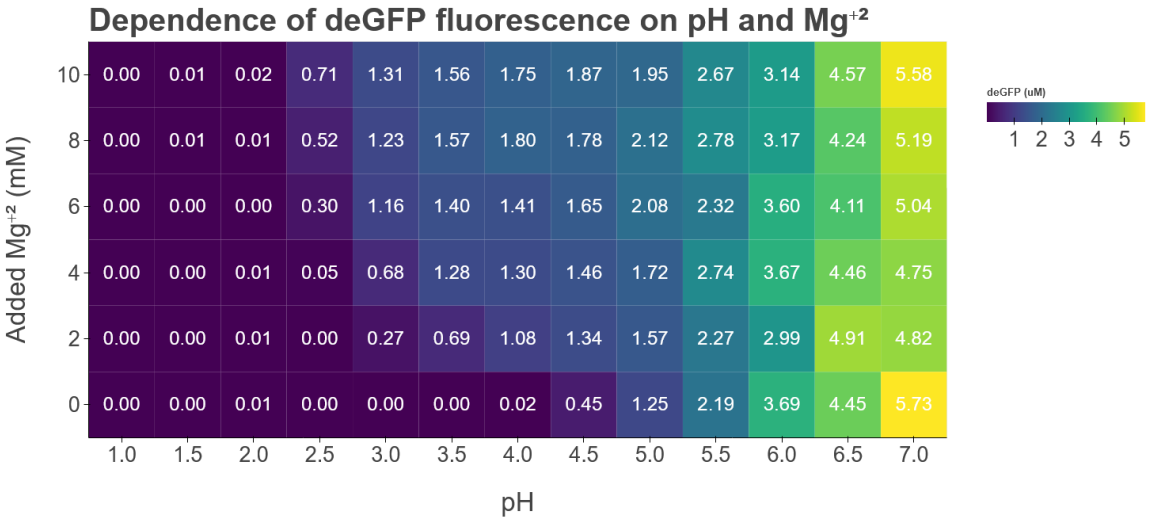

(b)

Figure A.3: Exploring the dependence of MGaptamer and deGFP fluorescence on pH and Mg^{+2} concentration. Either 0.2μM MGaptamer-deGFP mRNA (a) or 6.02μM deGFP (b) was added to 9uL of PBS of the appropriate pH, some amount of 100mM Mg-glutamate to the appropriate concentration, and nuclease-free water to 10μL. The 384-well plate was incubated for 18 hours in a plate-reader at 30°C, and the endpoint concentrations, as determined by the fluorescence calibration data, are indicated in the plots shown.

While it was not clear what change in cell-free metabolism would affect fluorescence would occur with increasing fuel concentration, a possible factor was pH, which has been shown in other studies to decrease over the course of a TX-TL reaction from about 7 to 5.5 at a standard concentration of 30mM 3-PGA [35].

The fluorescence of MGaptamer does not change over the relevant reaction conditions, nor is there a strong dependence on Mg^{+2} concentration at a given pH. Meanwhile, deGFP fluorescence depends strongly on pH and Mg^{+2}, even for the relevant reaction conditions, although fluorescence is consistent across Mg^{+2} concentration at a given pH. The experimental data shown in the main text suggest that endpoint deGFP concentration (or rather, fluorescence) is highest at low Mg^{+2} and medium to high fuel concentrations. Increasing fuel concentrations should result in decreased pH, at which there should be decreased fluorescence, which is not what is observed experimentally. These data seem to suggest that changing pH conditions are not sufficient to explain increased deGFP fluorescence at low Mg^{+2} and medium to high fuel concentrations, and that this increased fluorescence is likely the result of increased deGFP protein expression.

Using 3-PGA, TX-TL reactions were performed without any DNA, after which purified deGFP was added after 18 hours. The results of this experiment are shown below.

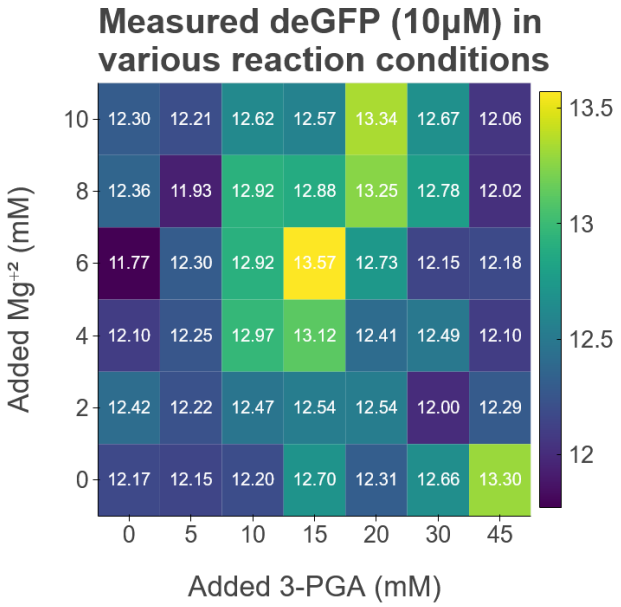

Figure A.4: Exploring the dependence of deGFP fluorescence on reaction conditions with varying Mg^{+2} and 3-PGA. 10μM purified deGFP was added to TX-TL reactions that had been incubated at 30°C for 18 hours. The final deGFP concentrations, as reported by the fluorescence values that were calibrated to micromolar units, are shown in the figure.

As shown in Fig. A.4, deGFP fluorescence is not affected in a predictable manner by Mg^{+2} and/or 3-PGA concentration in the experimental conditions explored in this work. However, there is an overall increase in fluorescence across all the experimental conditions.

A.4 Initial ideas and early experiments: titrations of TX-TL components

In the first set of experiments, TX-TL reactions were implemented with all components fixed (relative to a "standard TX-TL composition" [28]) except for the components of interest. These components of interest were the following:

- 3-PGA, used to regenerate energy;
- NTPs, used to generate mRNA and to provide energy for TX-TL;
- ATP, which provides energy for transcription and translation elongation;
- GTP, which provides energy for translation initiation;
- inorganic phosphate (P_i), a byproduct of 3-PGA metabolism that has been identified as a potential waste molecule by previous studies [18, 3];
- Mg^{+2}, whose chelation by P_i is a proposed mechanism by which TX-TL lifetime is limited [18], and thus the addition of which should improve protein yields;
- and NAD^+, another vital energy molecule but which previous studies have found does not significantly affect TX-TL [1, 4].

These components were titrated at 0%, 25%, 50%, 150%, and 200% of their standard concentrations, except for P_i, which was added at 1.25-5mM, where the upper range was set by the concentration of total NTPs (a source of P_i generation during TX-TL) used in a standard TX-TL reaction. The endpoint deGFP yields obtained from these reactions are shown below (Fig. A.5).

Most of these components were already at or near their optimal concentration for deGFP expression, compared to a positive control. As expected, NAD^+ concentrations did not significantly affect TX-TL. Meanwhile, both 3-PGA and Mg^{+2} concentrations drastically affected TX-TL, albeit both mostly reduced deGFP yields if varied. The plots suggest that having 50% less 3-PGA or 50% more Mg^{+2} may slightly improve TX-TL yields, although these slight differences are within range of experimental error. Increasing the concentration of NTP or ATP did not appreciably affect deGFP yield, but doubling the amount of GTP doubled deGFP yields.

While this initial round of experiments did not appreciably improve TX-TL performance (either by improving yields or prolonging lifetime – data not shown), it did reveal new and interesting

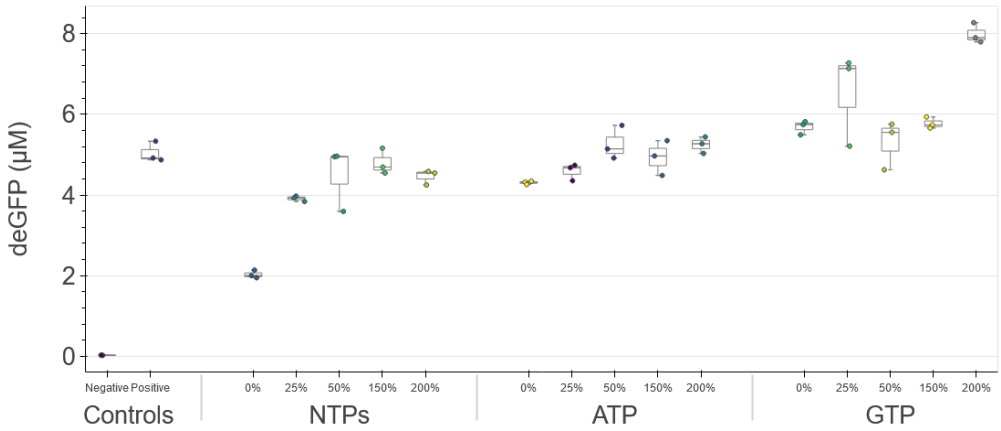

(a) NTP titrations

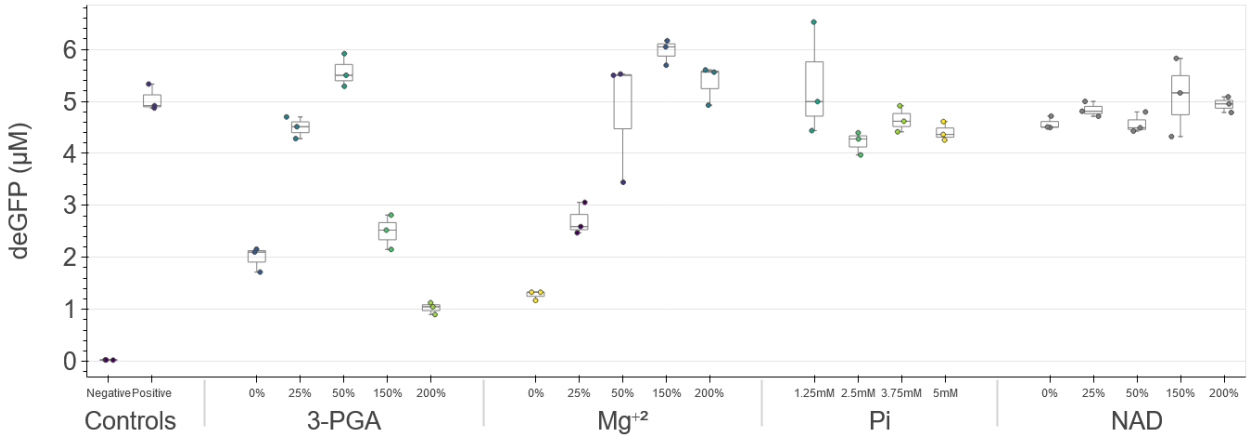

(b) Fuel and waste titrations

Figure A.5: Endpoint deGFP concentrations obtained after titration of TX-TL reaction components and subsequent reaction incubation for 14 hours. (a) NTP titrations were experiments where the concentration of ATP, GTP, or total NTPs was varied from the standard reaction set-up. (b) Fuel and waste titrations were experiments where concentration of 3-PGA, Mg, or NAD^+ was varied from the standard reaction set-up, or where P_i was added at low concentrations.

insights relevant to the cell-free metabolism model. The first revelation was the fact that TX-TL yields were high even when added 3-PGA was reduced significantly. Protein expression was possible even in the absence of energy regeneration by 3-PGA. These data suggested that alternative energy regeneration mechanisms may need to be included in a more accurate model of cell-free metabolism, and that similar deGFP yields may be achieved at different concentrations of 3-PGA when TX-TL machinery (RNA polymerases, ribosomes, etc.) is limited by the amount of DNA, mRNA, energy, or other resources in the system.

The second insight was that increasing the Mg^{+2} concentration by 50% slightly improved deGFP yields. This was especially peculiar because each batch of cell lysate is subjected to a salt calibration,

where TX-TL reactions are performed at several pairwise combinations of magnesium glutamate and potassium glutamate and optimal concentrations are determined and set for future experiments. In other words, the TX-TL reaction should already have been at the optimal Mg^{+2} concentration to start with. The only difference between the salt calibration experiments and these experiments was the concentration of DNA plasmid (encoding the mRNA sequence for deGFP) used; the former used 1nM DNA while the latter used 2.4nM DNA. TX-TL formulations used by other labs either also perform a salt calibration at a single concentration of DNA or don't perform salt calibrations at all (i.e. Mg^{+2} concentration is the same even for different batches of cell lysate). This raised a few questions: does Mg^{+2} affect TX-TL directly in addition to its effect on cell-free metabolism? More importantly, how might this effect be better modelled or understood to improve TX-TL performance?

The final insight was the finding that increasing the concentration of all NTPs or ATP was benign or harmful for TX-TL reactions, but increasing the concentration of GTP alone may be beneficial. However, it was not clear whether this was because the reaction was performed in a translation-limited system (where adding more GTP would increase the rate of translation initiation) or whether adding more GTP, which can be converted to ATP as needed by the enzyme Nucleoside diphosphate kinase (Ndk), provided a slowly-metabolized source of ATP that prevented the latter from being rapidly consumed by metabolic processes competing with TX-TL. It is worth noting here that the nucleotide composition of the mRNA encoding for deGFP is roughly 25% ATP, 27% GTP, 32% CTP, and 16% UTP; in other words, the sequence is not heavily biased towards GTP, which leads us to reject the hypothesis that the experimentally observed phenomenon is unique to this mRNA sequence or transcription-limited.

Taken together, these insights suggested the presence of interesting phenomenon involving fuel and energy metabolism, with a possible role for Mg^{+2} present as well. Subsequent experiments were aimed at further exploring these insights.

A.5 Exploring the effects of NTPs on TX-TL

Preliminary data showed that 3-PGA was not necessary for TX-TL, and that adding sufficient NTPs could recover TX-TL function for a given DNA concentration. However, could all NTPs be treated the same? Specifically, how did GTP and ATP uniquely affect TX-TL?

For these set of experiments, TX-TL reactions were set up without any 3-PGA or other fuel, and an NTP versus GTP versus ATP panel was performed. Each reagent was added at 0mM, 5mM, 10mM, or 15mM, and the NTP solution used consisted of 31.25% each of ATP and GTP, and 18.75% each of CTP and UTP. As the NTP solution also contained ATP and GTP, plots were constructed of total ATP versus total GTP, the results of which are shown below.

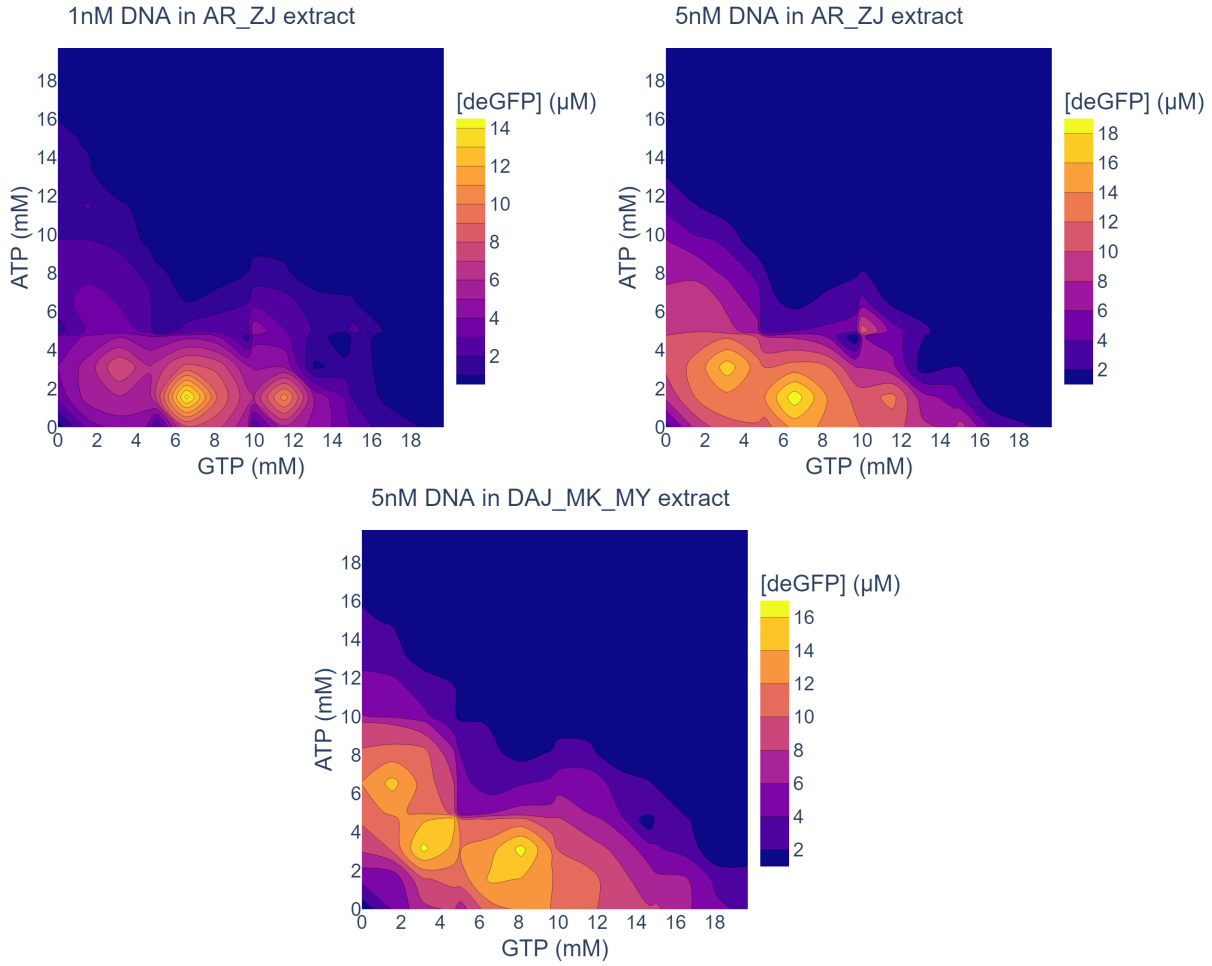

Figure A.6: Endpoint deGFP measurements for three different NTP versus GTP versus ATP screens, where total ATP versus total GTP is plotted. From top left to bottom, three different experimental conditions were used: (1) **AR_ZJ** lysate with 1nM DNA, (2) **AR_ZJ** lysate with 5nM DNA, and (3) **DAJ_MK_MY** lysate with 5nM DNA. Three biological replicates were used for each experimental condition, and the mean fluorescence value of each condition is in the panels above.

The plots indicate that high deGFP yields can be achieved for higher than standard (i.e. 1.5mM) concentrations of ATP or GTP. For the **AR_ZJ** lysate, adding more GTP was more beneficial than adding more ATP, but for the **DAJ_MK_MY** lysate, adding either more ATP or more GTP was equivalent in terms of endpoint deGFP yield. For all lysates, adding too much total NTPs resulted in decreased endpoint deGFP yields.

Attempts to gain a stronger biochemical understanding of this system through high-performance liquid chromatography and ion chromatography were unsuccessful, as the limit of detection is not low enough for detecting accurate concentrations of, and distinguishing between different states of, NTPs. Efforts are currently ongoing to use liquid chromatography-mass spectrometry (LC-MS) to obtain dynamic, accurate quantitative measurements of NTPs, NDPs, and NMPs. However, due to difficulty in measuring NTP dissipation to background metabolic processes versus interconversion among NTPs, these experiments and analysis are out of the scope of the current project.

A.6 Mg^{+2} vs. Fuel panels for alternative fuels

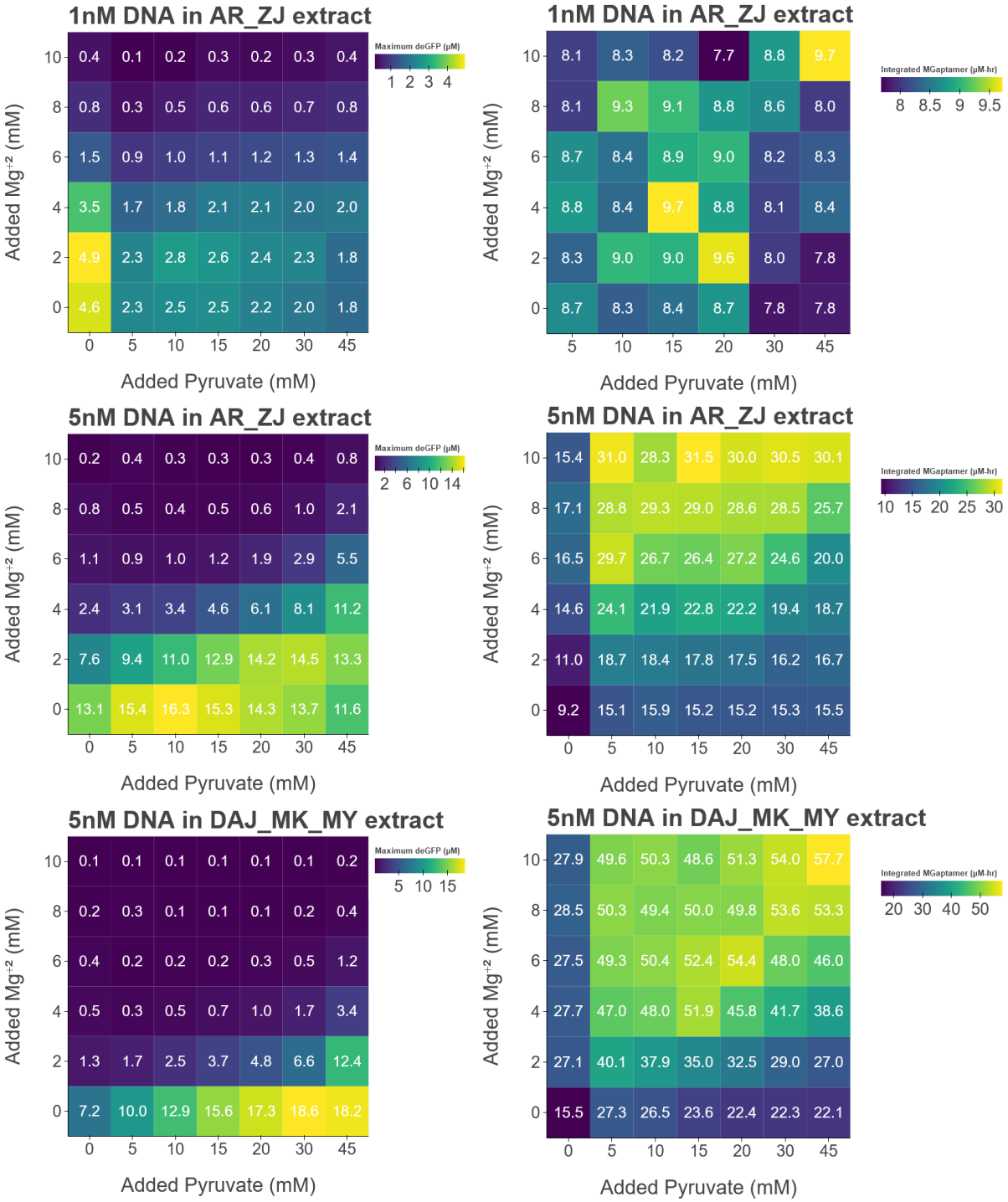

(a) deGFP endpoint measurements

(b) Integrated mRNA measurements

Figure A.7: Mg^{+2} vs. Pyruvate screens: endpoint deGFP and integrated mRNA measurements for three different experimental conditions. From top to bottom, three different experimental conditions were used: (1) **AR_ZJ** lysate with 1nM DNA, (2) **AR_ZJ** lysate with 5nM DNA, and (3) **DAJ_MK_MY** lysate with 5nM DNA. Three biological replicates were used for each experimental condition.

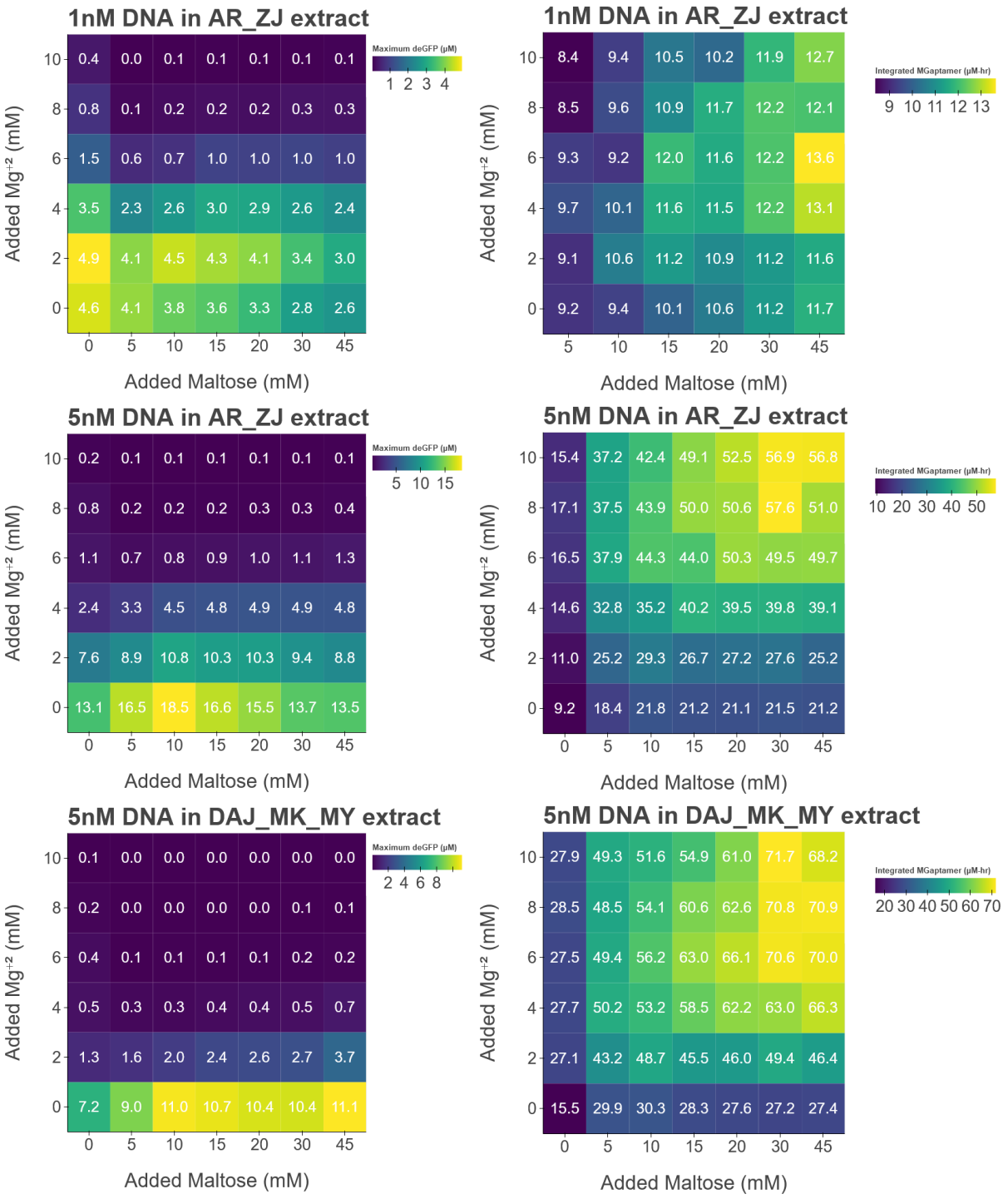

(a) deGFP endpoint measurements

(b) Integrated mRNA measurements

Figure A.8: Mg^{+2} vs. Maltose screens: endpoint deGFP and integrated mRNA measurements for three different experimental conditions. From top to bottom, three different experimental conditions were used: (1) **AR_ZJ** lysate with 1nM DNA, (2) **AR_ZJ** lysate with 5nM DNA, and (3) **DAJ_MK_MY** lysate with 5nM DNA. Three biological replicates were used for each experimental condition.

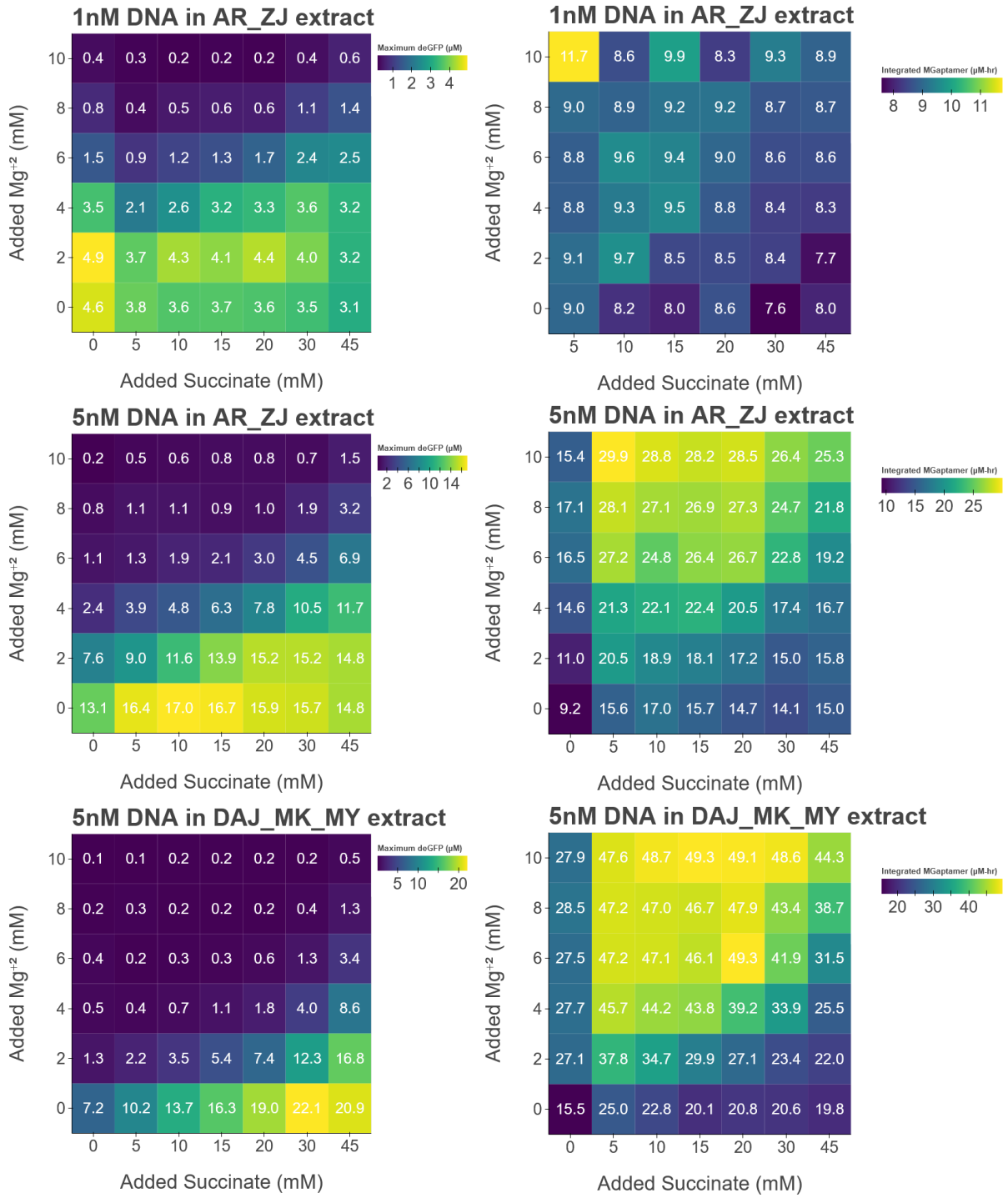

(a) deGFP endpoint measurements

(b) Integrated mRNA measurements

Figure A.9: Mg^{+2} vs. Succinate screens: endpoint deGFP and integrated mRNA measurements for three different experimental conditions. From top to bottom, three different experimental conditions were used: (1) **AR_ZJ** lysate with 1nM DNA, (2) **AR_ZJ** lysate with 5nM DNA, and (3) **DAJ_MK_MY** lysate with 5nM DNA. Three biological replicates were used for each experimental condition.

A.7 Trade-off curves with points colored by fuel concentration and fuel type

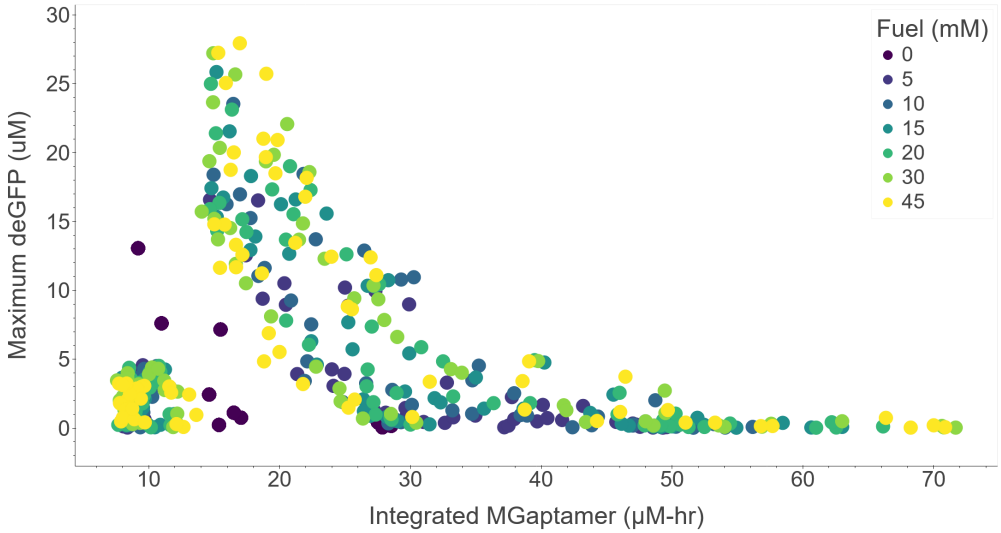

(a) Points colored by fuel concentration

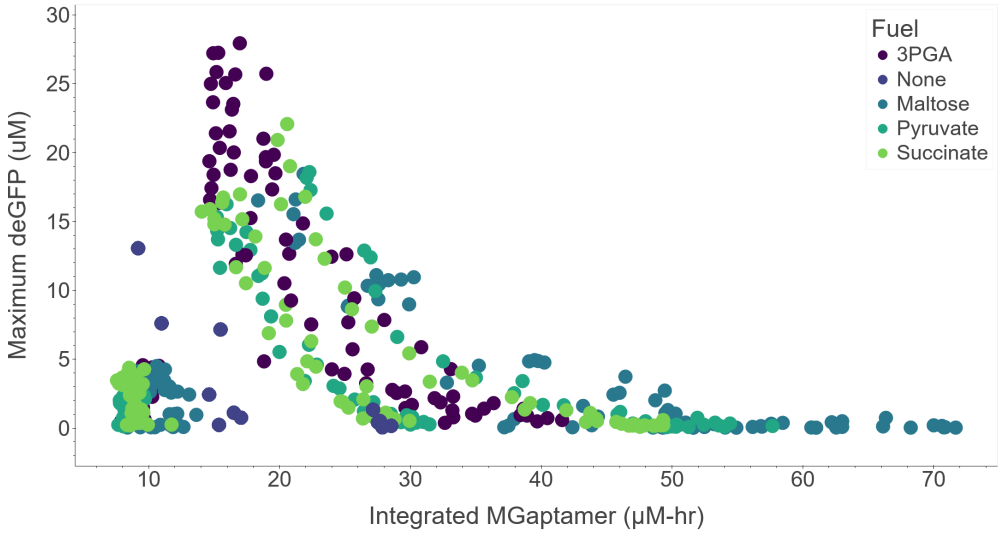

(b) Points colored by fuel type

Figure A.10: Endpoint deGFP concentrations versus integrated MGaptamer fluorescence. Each point represents an individual sample, colored by either (a) fuel concentration or (b) fuel type.

A.8 Trade-off curves with points colored by cell lysate batch

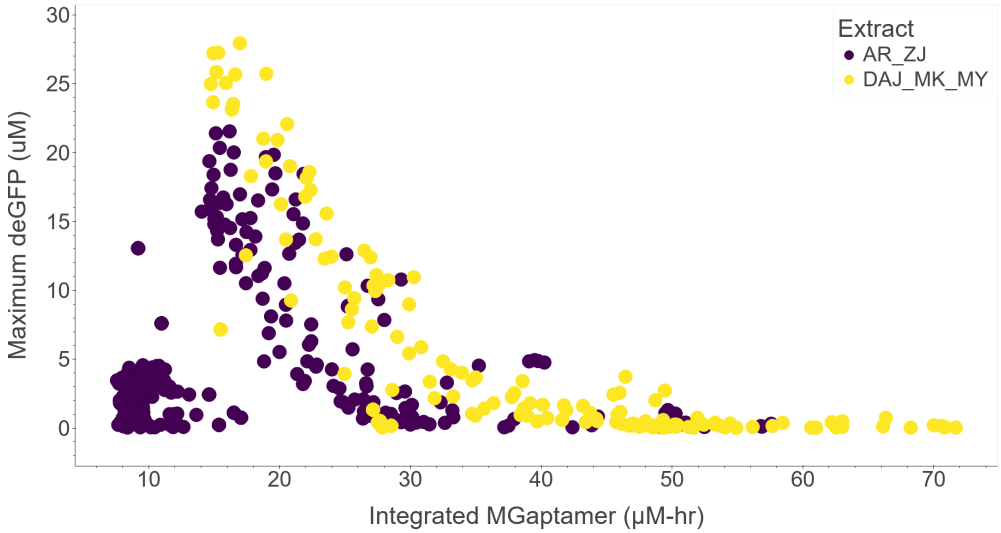

Figure A.11: Endpoint deGFP concentrations versus integrated MGaptamer fluorescence where points are colored by the batch of cell lysate used for that experiment. Each point represents an individual sample. Three different experimental conditions were overlaid for each plot: (1) **AR_ZJ** lysate with 1nM DNA, (2) **AR_ZJ** lysate with 5nM DNA, and (3) **DAJ_MK_MY** lysate with 5nM DNA. Three biological replicates were used for each experimental condition.

A.9 Trade-off curves separated by fuel source with points colored by Mg^{+2} concentration

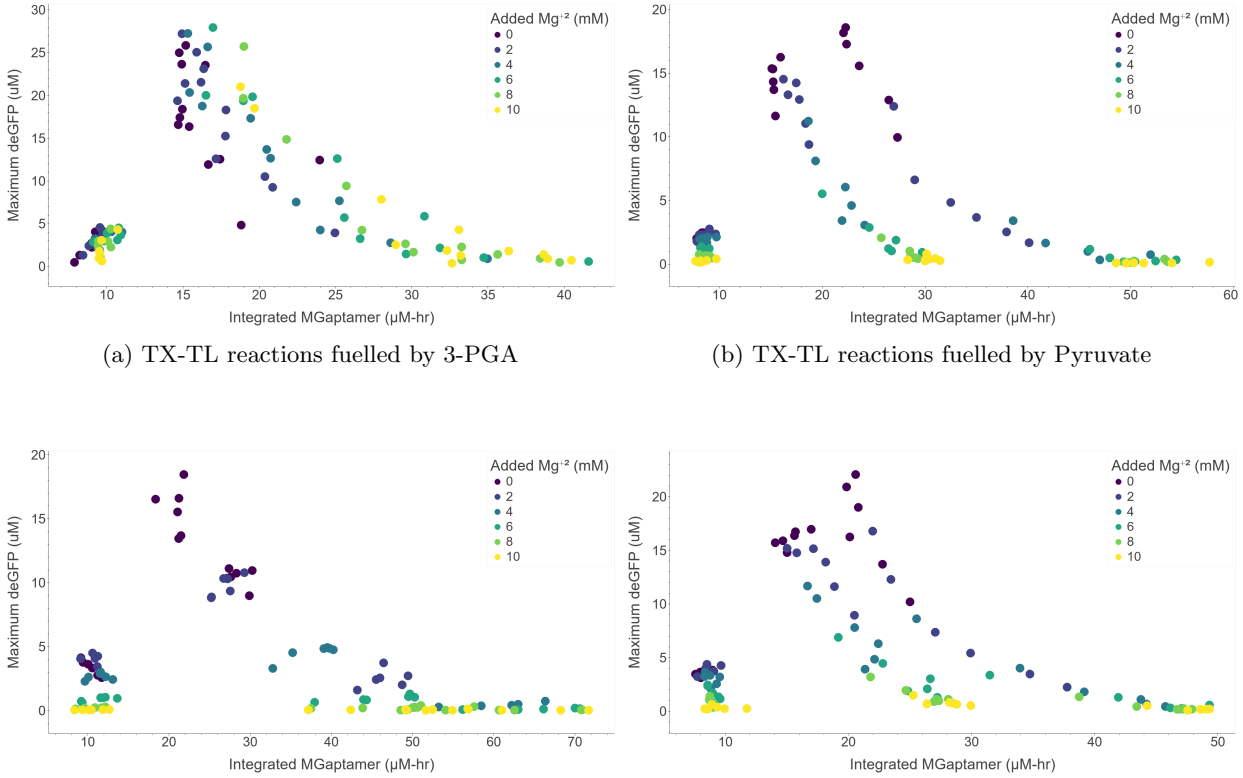

(a) TX-TL reactions fuelled by 3-PGA

(b) TX-TL reactions fuelled by Pyruvate

(c) TX-TL reactions fuelled by Maltose

(d) TX-TL reactions fuelled by Succinate

Figure A.12: Endpoint deGFP versus integrated mRNA measurements where plots are separated by fuel source and points are colored by Mg^{+2} concentration. Three different experimental conditions were overlaid for each plot: (1) **AR_ZJ** lysate with 1nM DNA, (2) **AR_ZJ** lysate with 5nM DNA, and (3) **DAJ_MK_MY** lysate with 5nM DNA. Three biological replicates were used for each experimental condition.

References

[1] Alice M. Banks, Colette J. Whitfield, Steven R. Brown, David A. Fulton, Sarah A. Goodchild, Christopher Grant, John Love, Dennis W. Lendrem, Jonathan E. Fieldsend, and Thomas P. Howard. Key reaction components affect the kinetics and performance robustness of cell-free protein synthesis reactions. *Computational and Structural Biotechnology Journal*, 20:218–229, Jan 2022.

[2] Victor Barrenechea, Maryhory Vargas-Reyes, Miguel Quiliano, and Pohl Milón. A complementary mechanism of bacterial mrna translation inhibition by tetracyclines. *Frontiers in Microbiology*, 12, 2021.

[3] Angelo C. Batista, Paul Soudier, Manish Kushwaha, and Jean-Loup Faulon. Optimising protein synthesis in cell-free systems, a review. *Engineering Biology*, 5(1):10–19, Mar 2021.

[4] Olivier Borkowski, Mathilde Koch, Agnès Zettor, Amir Pandi, Angelo Cardoso Batista, Paul Soudier, and Jean-Loup Faulon. Large scale active-learning-guided exploration for in vitro protein production optimization. *Nature Communications*, 11(1):1872, Apr 2020.

[5] August Brookwell, Javin P. Oza, and Filippo Caschera. Biotechnology applications of cell-free expression systems. *Life*, 11(12), 2021.

[6] Filippo Caschera, Ashty S. Karim, Gianluca Gazzola, Anne E. d'Aquino, Norman H. Packard, and Michael C. Jewett. High-throughput optimization cycle of a cell-free ribosome assembly and protein synthesis system. *ACS Synthetic Biology*, 7(12):2841–2853, Dec 2018.

[7] Fabio Chizzolini, Michele Forlin, Noël Yeh Martín, Giuliano Berloffa, Dario Cecchi, and Sheref S. Mansy. Cell-free translation is more variable than transcription. *ACS Synthetic Biology*, 6(4):638–647, Apr 2017.

[8] Eunhee Cho and Yuan Lu. Compartmentalizing cell-free systems: Toward creating life-like artificial cells and beyond. *ACS Synthetic Biology*, 9(11):2881–2901, Nov 2020.

[9] Stephanie D. Cole, Kathryn Beabout, Kendrick B. Turner, Zachary K. Smith, Vanessa L. Funk, Svetlana V. Harbaugh, Alvin T. Liem, Pierce A. Roth, Brian A. Geier, Peter A. Emanuel,

Scott A. Walper, Jorge L. Chávez, and Matthew W. Lux. Quantification of interlaboratory cell-free protein synthesis variability. *ACS Synthetic Biology*, 8(9):2080–2091, Sep 2019.

[10] Jonathan Garamella, Ryan Marshall, Mark Rustad, and Vincent Noireaux. The all e. coli tx-tl toolbox 2.0: A platform for cell-free synthetic biology. *ACS Synthetic Biology*, 5(4):344–355, Apr 2016.

[11] David Garenne, Matthew C. Haines, Eugenia F. Romantseva, Paul Freemont, Elizabeth A. Strychalski, and Vincent Noireaux. Cell-free gene expression. *Nature Reviews Methods Primers*, 1(1):49, Jul 2021.

[12] Nicole E. Gregorio, Max Z. Levine, and Javin P. Oza. A user's guide to cell-free protein synthesis. *Methods and protocols*, 2(1), Mar 2019.

[13] Nicholas Horvath, Michael Vilkhovoy, Joseph A. Wayman, Kara Calhoun, James Swartz, and Jeffrey D. Varner. Toward a genome scale sequence specific dynamic model of cell-free protein synthesis in escherichia coli. *Metabolic Engineering Communications*, 10:e00113, Jun 2020.

[14] Nan Jiang, Xuanwei Ding, and Yuan Lu. Development of a robust escherichia coli-based cell-free protein synthesis application platform. *Biochemical Engineering Journal*, 165:107830, Jan 2021.

[15] Ashty S. Karim, Quentin M. Dudley, Alex Juminaga, Yongbo Yuan, Samantha A. Crowe, Jacob T. Heggestad, Shivani Garg, Tanus Abdalla, William S. Grubbe, Blake J. Rasor, David N. Coar, Maria Torculas, Michael Krein, FungMin (Eric) Liew, Amy Quattlebaum, Rasmus O. Jensen, Jeffrey A. Stuart, Sean D. Simpson, Michael Köpke, and Michael C. Jewett. In vitro prototyping and rapid optimization of biosynthetic enzymes for cell design. *Nature Chemical Biology*, 16(8):912–919, Aug 2020.

[16] Ashty S. Karim, Jacob T. Heggestad, Samantha A. Crowe, and Michael C. Jewett. Controlling cell-free metabolism through physiochemical perturbations. *Metabolic Engineering*, 45:86–94, Jan 2018.

[17] Richard Kelwick, Alexander J. Webb, James T. MacDonald, and Paul S. Freemont. Development of a bacillus subtilis cell-free transcription-translation system for prototyping regulatory elements. *Metabolic Engineering*, 38:370–381, Nov 2016.

[18] Tae-Wan Kim, Dong-Myung Kim, and Cha-Yong Choi. Rapid production of milligram quantities of proteins in a batch cell-free protein synthesis system. *Journal of Biotechnology*, 124(2):373–380, Jul 2006.

[19] April M. Miguez, Yan Zhang, Fernanda Piorino, and Mark P. Styczynski. Metabolic dynamics in escherichia coli-based cell-free systems. *ACS Synthetic Biology*, 10(9):2252–2265, Sep 2021.

[20] Vijayalakshmi H Nagaraj, James M Greene, Anirvan M Sengupta, and Eduardo D Sontag. Translation inhibition and resource balance in the tx-tl cell-free gene expression system. *Synthetic Biology*, 2(1):ysx005, Jan 2017.

[21] Peter Q. Nguyen, Luis R. Soenksen, Nina M. Donghia, Nicolaas M. Angenent-Mari, Helena de Puig, Ally Huang, Rose Lee, Shimyn Slomovic, Tommaso Galbersanini, Geoffrey Lansberry, Hani M. Sallum, Evan M. Zhao, James B. Niemi, and James J. Collins. Wearable materials with embedded synthetic biology sensors for biomolecule detection. *Nature Biotechnology*, 39(11):1366–1374, Nov 2021.

[22] William Poole. *Compilation and Inference with Chemical Reaction Networks*. Thesis, California Institute of Technology, 2021.

[23] Katherine A Rhea, Nathan D McDonald, Stephanie D Cole, Vincent Noireaux, Matthew W Lux, and Patricia E Buckley. Variability in cell-free expression reactions can impact qualitative genetic circuit characterization. *Synthetic Biology*, 7(1):ysac011, Jan 2022.

[24] Ankita Roychoudhury. *Understanding the lifetime and rate of protein production in cell-free reactions while maximizing energy use*. Undergraduate thesis, California Institute of Technology, 2021.

[25] Caitlin E. Sharpes, John B. McManus, Steven M. Blum, Glory E. Mgboji, and Matthew W. Lux. Assessment of colorimetric reporter enzymes in the pure system. *ACS Synthetic Biology*, 10(11):3205–3208, Nov 2021.

[26] Yoshihiro Shimizu, Akio Inoue, Yukihide Tomari, Tsutomu Suzuki, Takashi Yokogawa, Kazuya Nishikawa, and Takuya Ueda. Cell-free translation reconstituted with purified components. *Nature Biotechnology*, 19(8):751–755, Aug 2001.

[27] Vipul Singhal. *Modeling, Computation, and Characterization to Accelerate the Development of Synthetic Gene Circuits in Cell-Free Extracts*. PhD thesis, California Institute of Technology, 2019.

[28] Zachary Z. Sun, Clarmyra A. Hayes, Jonghyeon Shin, Filippo Caschera, Richard M. Murray, and Vincent Noireaux. Protocols for implementing an escherichia coli based tx-tl cell-free expression system for synthetic biology. *JoVE*, (79):e50762, Sep 2013.

[29] Zoe Swank and Sebastian J. Maerkl. Cfpu: A cell-free processing unit for high-throughput, automated in vitro circuit characterization in steady-state conditions. *BioDesign Research*, 2021:2968181, Mar 2021.

[30] Melissa K. Takahashi, Clarmyra A. Hayes, James Chappell, Zachary Z. Sun, Richard M. Murray, Vincent Noireaux, and Julius B. Lucks. Characterizing and prototyping genetic networks with cell-free transcription–translation reactions. *Bacterial and Archaeal Transcription*, 86:60–72, Sep 2015.

[31] Francois-Xavier Theillet, Andres Binolfi, Tamara Frembgen-Kesner, Karan Hingorani, Mohona Sarkar, Ciara Kyne, Conggang Li, Peter B. Crowley, Lila Gierasch, Gary J. Pielak, Adrian H. Elcock, Anne Gershenson, and Philipp Selenko. Physicochemical properties of cells and their effects on intrinsically disordered proteins (idps). *Chemical Reviews*, 114(13):6661–6714, Jul 2014.

[32] Grace E. Vezeau and Howard M. Salis. Tuning cell-free composition controls the time delay, dynamics, and productivity of tx-tl expression. *ACS Synthetic Biology*, 10(10):2508–2519, Oct 2021.

[33] Michael Vilkhovoy, Nicholas Horvath, Che-Hsiao Shih, Joseph A. Wayman, Kara Calhoun, James Swartz, and Jeffrey D. Varner. Sequence specific modeling of e. coli cell-free protein synthesis. *ACS Synthetic Biology*, 7(8):1844–1857, Aug 2018.

[34] Bastian Vögeli, Luca Schulz, Shivani Garg, Katia Tarasava, James M. Clomburg, Seung Hwan Lee, Aislinn Gonnot, Elamar Hakim Moully, Blaise R. Kimmel, Loan Tran, Hunter Zeleznik, Steven D. Brown, Sean D. Simpson, Milan Mrksich, Ashty S. Karim, Ramon Gonzalez, Michael Köpke, and Michael C. Jewett. Cell-free prototyping enables implementation of optimized reverse beta-oxidation pathways in heterotrophic and autotrophic bacteria. *Nature Communications*, 13(1):3058, Jun 2022.

[35] Yiran Wang and Y-H Percival Zhang. Cell-free protein synthesis energized by slowly-metabolized maltodextrin. *BMC Biotechnology*, 9(1):58, Jun 2009.

[36] N. Amy Yewdall, Alexander F. Mason, and Jan C. M. van Hest. The hallmarks of living systems: towards creating artificial cells. *Interface Focus*, 8(5):20180023, Oct 2018.

[37] Yan Zhang, Paige L. Steppe, Maxwell W. Kazman, and Mark P. Styczynski. Point-of-care analyte quantification and digital readout via lysate-based cell-free biosensors interfaced with personal glucose monitors. *ACS Synthetic Biology*, 10(11):2862–2869, Nov 2021.